ORNL/TM-2018/912

Handbook of LWR SiC/SiC Cladding Properties - Revision 1

Nuclear Technology Research and Development

Prepared for
U.S. Department of Energy
Nuclear Technology Research and Development Advanced Fuels Campaign

T. Koyanagi[1], Y. Katoh[1]
G. Jacobsen[2], C. Deck[2]
[1]Oak Ridge National Laboratory
[2]General Atomics

August 2018
M2NT-18OR020202101

SUMMARY

This report aims to provide properties data of silicon carbide (SiC) fiber–reinforced SiC matrix (SiC/SiC) composites for use in modeling for their application as accident-tolerant fuel cladding for light water reactors (LWRs). The properties data presented are specifically for geometries relevant to fuel cladding tubes, although many properties can be derived or predicted based on data from planar geometry specimen data. This report presents various properties, including mechanical properties, thermal properties, chemical stability under normal and off-normal operation conditions, hermeticity, and irradiation resistance. Table S.1 provides a high level summary of those properties mainly for nuclear-grade SiC/SiC composites fabricated via a chemical vapor infiltration (CVI) route, which has been updated from the previous report (ORNL/TM-2017/385). The newly added data include statistical tensile properties, hydrothermal corrosion behavior of environmental barrier coating on SiC, and accurate temperature- and dose-dependent swelling of SiC/SiC composites. Table S.1 includes high level comments about reliability of properties data with an intention to assist proper performance modeling. While most of the important properties are available, this work also identified remaining critical data gap, including data for the in-pile hydrothermal corrosion, accurate thermal properties of tubular components, and anisotropic elastic properties.

Table S.1. Property summary of CVI SiC/SiC fuel cladding tubes for LWR applications. The typical tube has outer diameter of ~10 mm and wall thickness of ~1.5 mm, and the direction of fiber reinforcement is ±30–60° orientation (0° indicates that the fiber axis corresponds to tube length direction). Note that the properties are representative for fully composite tubes without additional layer or layers of thick monolithic SiC or non-SiC materials, unless otherwise indicated.

Properties	Nonirradiated	Neutron-irradiated
Density	~2.7 g/cm^3	Temperature and dose dependent swelling (Eq. (6)) Reliable data obtained from flat coupons
Porosity	10–15%	No irradiation effect
Fiber volume fraction	30–40 %	No irradiation effect
Coefficient of thermal expansion	Eq. (1) Reliable data obtained from flat coupons	No change by irradiation until swelling starts to be annealed beyond irradiation temperature (Proved using flat coupons)
Thermal diffusivity	Table 5 Lacking extensive data base and high-fidelity model	Estimated from data obtained from flat coupons (Figure 17) Lacking extensive data base and high-fidelity model
Specific heat	Figure 4 Assumed to be same as CVD SiC	No change expected until stored energy starts to be released
Gas leak tightness	Leak tight, relying on intact overcoat layer of SiC Gas permeation through crack networks is a probabilistic phenomenon: limited data in Table 6	Overcoat SiC layer is leak tight following neutron irradiation Potential crack network development during operation has not been evaluated
Elastic constants	Young's modulus: 129–248 GPa (axial), 160–215 GPa (hoop). Significant dependence on architecture. Other elastic constants; Figure 6 (Limited data available for anisotropic elastic constants)	Slight reduction in modulus; Figure 20 Reliable data obtained from flat coupons
Proportional limit stress	80–100 MPa (axial); ~100 MPa (hoop)	Insignificant irradiation effect expected from results of flat coupons
Ultimate strength	Figure 7 (axial tensile) and Figure 8 (hoop tensile)	Insignificant irradiation effect expected from results of flat coupons
Statistical strength	Limited data in Section 3.2.5. Data needed for specific composites or components.	No change assumed for modeling based on limited data with flat coupons
Creep	Negligible thermal creep below ~1000°C	Negligible irradiation creep strain compared with swelling based on testing monolith and fibers Data needed for SiC/SiC composites for confirmation
Stored energy	Not applicable	Limited data available
Hydrothermal corrosion	Water chemistry–dependent mass loss (Figure 10)	Limited in-pile data available
Compatibility with fuel	Insignificant SiC-UO_2 reaction under a normal operation condition	Expected insignificant reaction under a normal operation condition
Steam oxidation	Orders of magnitude lower steam oxidation rates than Zr	Expected negligible irradiation effect

This page is intentionally left blank.

CONTENTS

FIGURES

TABLES

ABBREVIATIONS, ACRONYMS, AND INITIALISMS

Acronym	Description	Acronym	Description
°C	Degree Celsius	LVDT	Linear variable differential transformer
2D	Two dimensional	LWR	Light water reactor
3D	Three dimensional	Li	Lithium
Ag	Silver	Mg	Magnesium
Al	Aluminum	MPa	Megapascal
ASTM	American Society for Testing and Materials	NITE	Nano-infiltration and transient eutectic phase
ATF	Accident tolerant fuels	O	Oxygen
B	Boron	OD	Outer diameter
C.V.	Coefficient of variance	PLS	Proportional limit stress
cm	Centimeter	PVD	Physical vapor deposition
CMC	Ceramic matrix composite	PyC	Pyrolytic carbon
Cu	Copper	Ref.	Reference
CVD	Chemical vapor deposition	SA3	Tyranno SA3
CVI	Chemical vapor infiltration	Si	Silicon
EBC	Environmental barrier coating	SiC	Silicon carbide
FCCI	Fuel-clad chemical interaction	Ti	Titanium
g	gram	UTS	Ultimate tensile strength
GPa	Gigapascal	VPS	Vacuum plasma spray
HNS	Hi-Nicalon Type S	Y	Yttrium
HS	hermetic sealing	Zr	Zirconium
ID	Inner diameter		

HANDBOOK OF LWR SIC/SIC CLADDING PROPERTIES – REVISION 1

1. INTRODUCTION

1.1 Background

Fuels and core structures in current light water reactors (LWRs) are vulnerable to catastrophic consequences in the event of certain loss of coolant scenarios that fall outside of the design basis of the plant, as was evidenced by the March 2011 Fukushima Dai-ichi Nuclear Power Plant accident [1]. This vulnerability is attributed primarily to the rapid oxidation kinetics of zirconium (Zr) alloys in a water vapor environment at very high temperatures, which results in the production of hydrogen and heat [1, 2]. Current LWRs use Zr alloys nearly exclusively as materials for fuel cladding and core structures. Silicon carbide (SiC)–based materials, in particular continuous SiC fiber–reinforced SiC matrix ceramic composites (SiC/SiC composites or SiC composites) are among the candidate alternative materials for LWR fuel cladding and certain core structures such as BWR channel box to enable so-called accident-tolerant fuels (ATFs) and accident-tolerant cores. SiC and SiC/SiC composites components are considered to provide outstanding passive safety features in beyond-design-basis severe accident scenarios [1, 2]. SiC/SiC composites are anticipated to provide additional benefits over Zr alloys: smaller neutron absorption cross sections, general chemical inertness, ability to withstand higher neutron doses and higher temperatures, lack of progressive irradiation growth, and low induced activation/low decay heat [3]. Moreover, SiC is considered to be permanently stable in nuclear waste [3]. Although SiC-based cladding appears to be attractive, critical feasibility issues such as (1) hydrothermal corrosion, (2) potential loss of fission gas retention due to cracking under normal operation conditions, (3) development of fuel performance modeling capability, and (4) fabrication of full length tube with sufficient quality, must be addressed [4, 6]. This report is related to the issue of modeling capability. For successful development of SiC-based cladding, such fuel performance modeling plays critical roles, as explained in Section 1.2.

1.2 Document Purpose

After decades of experience with metallic cladding components in thermal and fast reactors, the transition to using SiC ceramic matrix composites represents a revolutionary paradigm shift. Because of the impact associated with any such transition, associated challenges will need to be carefully assessed via predictive fuel performance analysis. Fuel performance analysis tools guide the design process to optimize performance for the integral fuel module under normal and off-normal operating conditions. Note that the term “fuel,” as used herein, refers to the integral structure consisting of the pellet, the cladding, and other fuel assembly components.

Although the properties of SiC/SiC composites, including the effects of neutron irradiation, are relatively well understood as a candidate fuel cladding material [5], they have been insufficiently incorporated in fuel performance models and core designs. There are several reasons for this, including the intrinsic behavioral differences between ceramic composites and metallic alloys, the tailorable and anisotropic nature of composite properties, and the complexity of interactions among irradiation-induced evolutions of thermophysical properties. To achieve improved fidelity for comprehensive performance modeling and analysis of fuel systems involving SiC/SiC cladding, properties of these composites in small-diameter tubular geometries are compiled and analyzed in this report. The properties data analysis and interpretation are discussed in relation to the constitutive modeling, effects of neutron irradiation, predictive capability, and critical deficiencies in data and knowledge.

The intent of this document is to summarize the material properties available for as-manufactured and irradiated SiC/SiC composite fuel cladding in the form of thin tubes. If data are not yet available, SiC/SiC plate data are given with an explanation on how it would apply to tubes.

1.3 Product Forms

The SiC/SiC composites analyzed in this report are limited to continuous and near-stoichiometric SiC fiber–reinforced composites with fully crystalline SiC matrices. The SiC/SiC composite–based fuel claddings that are currently considered for LWRs include fully ceramic composite cladding, layered cladding consisting of any combination of SiC composite and monolithic SiC layers, and a variety of ceramic–metal hybrid concepts that use SiC/SiC composites as the primary structural element and a compliant metal to aid in fission product retention (see Table 1 for examples). Other functions of these layers include hermetic sealing (HS) and environmental barrier coatings (EBCs). Note that the properties provided in this report are representative for fully composite tubes without additional layer or layers of thick monolithic SiC or non-SiC materials, unless otherwise indicated.

Table 1. Examples of SiC/SiC composite configurations

Class	Layer configuration (from inner to outer)	Configuration	Remarks	Reference
Full ceramics	Composite		Monolithic surface layer may present	[6]
	Composite-monolith	Duplex	Monolithic layer as HS/EBC against hydrothermal corrosion	[7]
	Monolith-composite	Duplex	Monolithic layer as HS/EBC against fuel-cladding chemical interaction (FCCI)	[6]
	Monolith-composite-monolith	Triplex	Monolithic layer as HS/EBC against hydrothermal corrosion and FCCI	[8]
Metal-assisted ceramics	Metal-composite	Duplex	Metallic layer as HS/EBC against FCCI	[9]
	Composite-metal	Duplex	Metallic layer as HS/EBC against hydrothermal corrosion	[10]
	Metal-composite-metal	Triplex	Metallic layer as HS/EBC against hydrothermal corrosion and FCCI	Not proposed
	Composite-metal-composite	Triplex	Metallic layer as HS	[11]

Multiple types of SiC/SiC cladding tubes are available, manufactured with different combinations of fibers, interphases, matrices, and architectures. Table 2 lists the SiC/SiC clad tubes under consideration for this material handbook.

Table 2. SiC/SiC tube configurations considered for material handbook

Type	Fiber	Interphase	Matrix
Type 1	HNS fiber	Pyrolytic carbon	Chemical vapor infiltrated (CVI) SiC
Type 2	SA3 fiber	Pyrolytic carbon	CVI SiC
Type 3	SA3 fiber	Pyrolytic carbon	Nano-infiltration and transient eutectoid SiC
Type 4	All tubes that do not fall under Types 1–3, e.g., IBN fiber		

1.4 Specifications and Standards

There is no standard manufacturing specification for SiC/SiC tubes because standards are still under development. ASTM C1783-15, "Standard Guide for Development of Specifications for Fiber Reinforced Silicon Carbide-Silicon Carbide Composite Structures for Nuclear Applications," is a guide for preparing material specifications for SiC/SiC composite structures (flat plates, rectangular bars, round-rods, and tubes) that are manufactured specifically for structural components and for fuel cladding in nuclear reactor core applications. This standard also recommends ASTM standards according to which the physical, mechanical, and durability properties should be measured.

2. DESIGN AND MANUFACTURE

The following are the general manufacturing steps for SiC/SiC cladding:

1. SiC fibers are braided/knitted/stitched into 3-dimensional (3D) tubes, referred to as the architecture of the tubes.
2. An interphase layer is added by chemical vapor deposition (CVD).
3. The matrix is added by either chemical vapor infiltration (CVI) or by nano-infiltration transient eutectic phase (NITE) sintering using hot pressing.
4. Inner or outer coating layers may be added using different techniques.

The composite properties are to a large extent determined by the volume fractions and orientations of the fibers in relation to the orientation of interest for certain properties [5]. The presence of inner and/or outer coating layers may have a significant impact on the properties depending on the coating thickness.

The following sections describe the design and manufacture of SiC/SiC composite fuel cladding. Their purpose is to give the reader some background to aid understanding of how each manufacturing component can influence the material properties of the final tube.

2.1 Fibers

2.1.1 Fiber type

Nuclear-grade SiC fiber is considered near-stoichiometric and highly crystalline because of its dimensional stability under irradiation compared with non-stoichiometric and amorphous-like SiC fibers [5, 12]. This generation III class of SiC fibers includes Hi-Nicalon Type S (HNS; NGS Advanced Fibers, Toyama, Japan), Tyranno SA3 (SA3; Ube Industries Ltd., Ube, Japan), and Sylramic-iBN (COI Ceramics, San Diego). The properties of these fibers can be found elsewhere [13]. Briefly, they have similar mechanical properties: Young's modulus of ~400 GPa and room temperature tensile strength of

>2 GPa, but their thermal properties may differ significantly. The effect of the fiber on the properties of the tube is highly dependent on the fiber architecture.

2.1.2 Fiber architecture

Given certain properties for the constituent materials, the composite properties are determined by the fiber architecture. The reinforcing fibers provide benefits such as strength and toughness most effectively in directions parallel to the fiber axis. More precisely, the composite properties are to a large extent determined by the volume fractions and orientations of the fibers in relation to the orientation of interest for certain properties. Therefore, tailoring the fiber architecture is a key to optimizing the cladding mechanical properties [5]. Examples of fiber architecture are shown in Figure 1.

The common fiber architectures include two direction (2D) layups in the form of woven fabrics, 2.5D layups with cross weaving through the woven fabrics, 3D orthogonal weaves. In addition, braiding (both 2D and 3D) preforms have become popular [11] because of the high level of conformability and damage resistance. 2D braided preforms are composed of intertwined fiber structures capable of 0° and ±θ layups. 3D braiding preforms are produced by intertwining or orthogonal interlacing of yarns to form an integral structure through position placement thereby providing through-thickness reinforcement as well as being readily adaptable to a wide range of complex shapes.

The different fiber architecture was reported to result in different fiber volume fraction and size and distribution of pores [11], which greatly affects the thermomechanical properties of the composites. The effects of fiber architecture on the mechanical properties are shown and discussed in section 3.2.

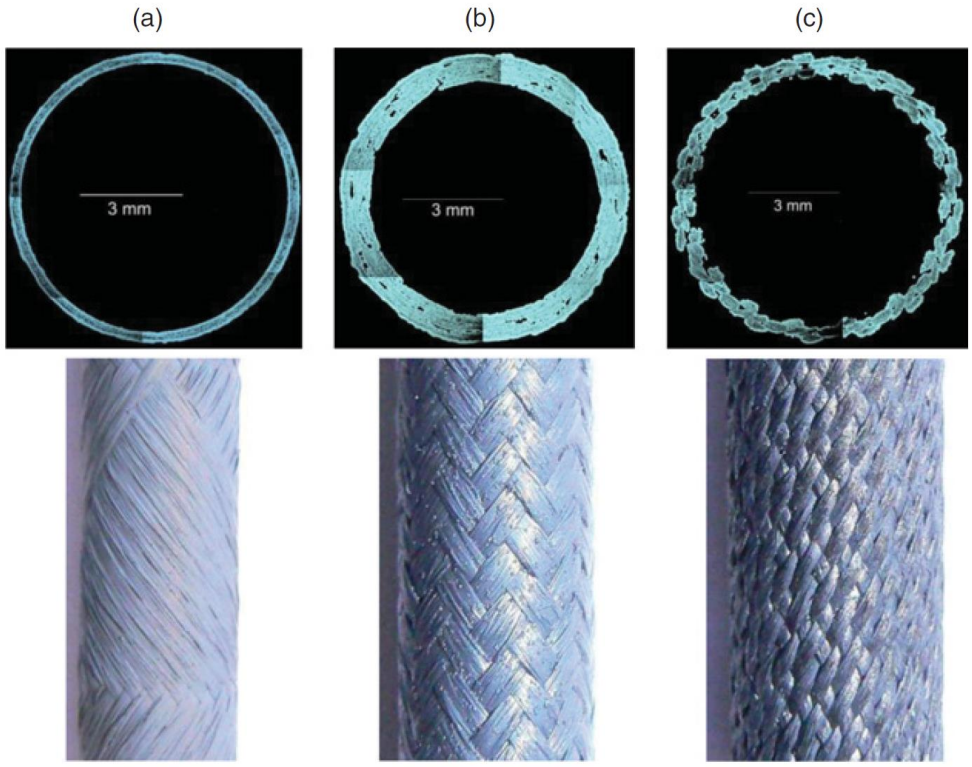

Figure 1. Examples of the fiber architecture of a CVI SiC/SiC tube: (a) filament winding, (b) 2D braiding, and (c) 3D braiding. Reprinted from Sauder 2014 [11].

2.2 Interphase

SiC/SiC composites are engineered materials particularly attractive for their tailorable, predictable, and reliable mechanical properties and excellent damage tolerance. The advantages of SiC/SiC composites are enabled by their fiber-matrix interface with adequate bonding strength and interfacial sliding strength. The primary tough fracture behavior of the ceramic composite is realized through the deflection of matrix cracks at the fiber/matrix interface without the breaking of fibers followed by fiber pull-out that is associated with frictional dissipation. Carbon-based interphases, such as the monolayer pyrolytic carbon (PyC) interphase and the multi-layer PyC/SiC interphase (Figure 2), are proven to be irradiation resistant [5]. The interphase is typically formed via a CVD process. The interphase thickness has been reported to slightly affect mechanical properties such as ultimate tensile strength (UTS), proportional limit stress (PLS), Young's modulus, and strain to failure when plate specimens were tested [14]. No systematic investigation of the effects of the interphase thickness on the mechanical properties of tubular SiC/SiC materials has been reported.

Boron nitride (BN) might be another option for the interphase material if isotropically controlled ^{11}BN is used to eliminate the ^{10}B content to avoid boron burnup and the production of transmutant helium by ^{10}B (n, a) ^{7}Li reactions during irradiation.

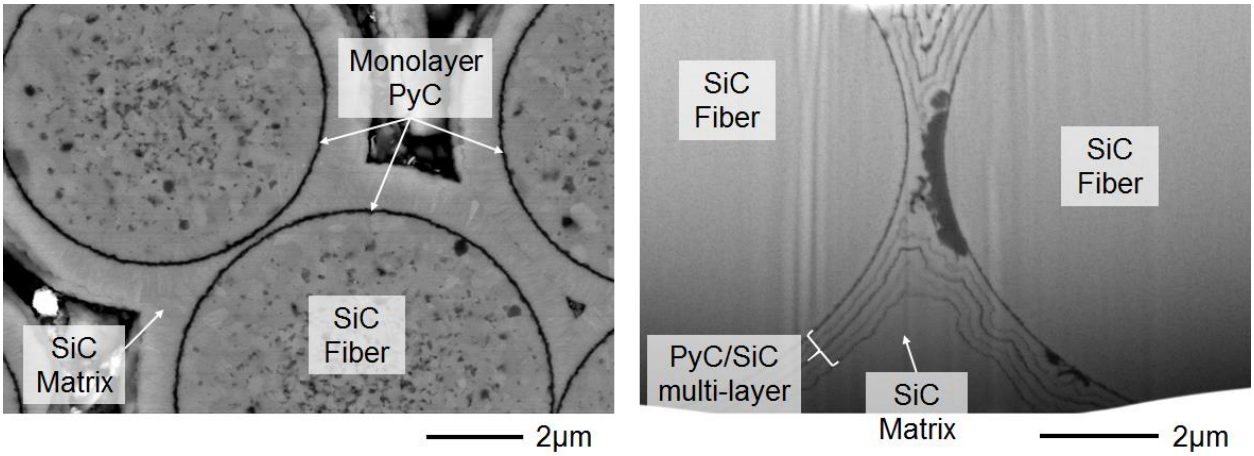

Figure 2. Examples of monolayer PyC interphase (left) and multilayer PyC interphase (right).

2.3 Matrix

SiC/SiC composite densification routes that have been proven to produce radiation-resistant forms of composite materials are CVI and SiC powder sintering represented by the NITE (nano-infiltration and transient eutectic phase) process. CVI SiC/SiC is a mature technology that has already demonstrated scale components with reasonable reproducibility up to large dimensions [15]. Experience with NITE SiC/SiC is more limited, but the fabrication of SiC/SiC composites of complex shapes—such as variable-diameter combustor liners, heat exchangers, and screw-ended tubes—has been demonstrated [16]. The manufacture of thin-walled tubes with a large length-to-diameter ratio remains a challenge for both fabrication routes.

2.3.1 CVI matrix

CVI is the most reliable method of producing a matrix composed of the very high-purity, crystalline SiC that is necessary to provide good irradiation resistance for nuclear applications [5]. For a CVI process,

manufacturing such tubes will require a large production facility that achieves adequate uniformity in temperature distribution and reactant flow conditions along the full tube length, which is technically not very difficult but will require a substantial capital investment.

The deposition rate is one of the key processing parameters. High deposition rates during composite fabrication leads to high levels of internal porosity. Low deposition rates are required to achieve low internal porosity, but they result in long fabrication times. Increasing the internal density of the matrix leads to improved mechanical and thermal properties [17].

General Atomics became capable of producing ~1 m long tubes via CVI with adequate straightness, wall thickness uniformity, roundness, and reproducibility of surface roughness [6]. Recently, General Atomics has produced a CVI furnace capable of manufacturing full length cladding. A Toshiba-Ibiden-Tohoku University team in Japan has developed a CVD/CVI facility that is capable of manufacturing prototype channel boxes and is in the process of expanding that process to manufacture full-length (~4 m) components.

Alternative methods for the manufacture of tubes with extreme length-to-diameter ratios, such as segmented tube fabrication, may also be considered. Options may include adhesive joining or mechanical fastening of shorter tubes to make full-length fuel rods, or modifying the fuel assembly design to accommodate axially stacked shorter fuel rods that are individually sealed.

2.3.2 NITE matrix

The NITE process has demonstrated an almost fully dense SiC/SiC composite [18]. This achievement is beneficial to the fabrication of a gas-leaktight cladding without any additional processing such as a CVD SiC coating. NITE is a specific type of liquid-phase sintering for SiC/SiC composites: sintering of SiC fiber forms infiltrated with a SiC slurry consisting of a SiC powder with nanosize particles and oxide additives allowing a eutectic composition of silica, alumina, and yttria [18]. NITE SiC/SiC tubes may be produced by a hot isostatic press, using a furnace of adequate size. A 20 cm long tube has been fabricated for irradiation in a material testing reactor [19].

Since the NITE matrix contains secondary phases attributed to the oxide additives, a key challenge for the LWR cladding application is achieving a matrix resistant to reactor environments, including hydrothermal corrosion for normal operation and high-temperature steam oxidation for accident conditions. The secondary phases along the grain boundaries and grain pockets are preferentially attacked under a hydrothermal corrosion environment [20].

2.4 Coatings

At normal operating conditions, depending on the water chemistry, SiC may corrode at an unacceptable rate. As a ceramic matrix composite material, it is expected to undergo microcracking under normal stress conditions, based on statistical probability; the cracking may compromise its ability to contain gaseous fission products. A possible solution to both issues is the application of mitigating coatings on the outer surface of the cladding for use in normal operating conditions. Such an environmental barrier coating (EBC) to prevent hydrothermal corrosion is being actively developed for Zr-based cladding [21]. For SiC/SiC composites, the EBC is a familiar way of improving high-temperature corrosion resistance for turbine applications [22]. However, there has been only limited development of EBCs for LWR SiC claddings. Coating technologies reported in the literature include electrochemical deposition of chromium; cathodic arc physical vapor–deposited Cr, CrN, and TiN; and vacuum plasma–sprayed Cr and Zr [10, 23]. Note that current EBC technology for ATF SiC/SiC cladding is immature, and future work should include demonstrations of hydrothermal corrosion resistance and hermeticity.

2.5 Joints

For the successful development of SiC-based fuel cladding, joining of the cladding to the end-plug is recognized as a technological hurdle [1]. This issue is specific to pin-type nuclear fission fuels. The functional requirements for the joint are (1) gas tightness to retain fission products inside the cladding; (2) environmental resistance, i.e., resistance to hydrothermal corrosion and neutron irradiation, under normal operating conditions; (3) high-temperature steam oxidation resistance under loss-of-coolant accident conditions; and (4) adequate mechanical properties. The performance of the joint is expected to be highly dependent on the bonding layer and the end-plug geometry.

The end-plug geometry may depend on the joining process and cladding material. Butted [24, 25], scarf [25], and butted scarf [25] end-plugs have been demonstrated. A screw type end-plug was employed in a case in which a machinable NITE SiC/SiC composite was used [19]. Generally, a larger bonding area yields superior mechanical properties, gas leak tightness, and corrosion/oxidation resistance. However, an end-plug and a cladding with relatively complex geometries will be required to achieve a radically larger bonding area.

There are various options for joining SiC to SiC, although limited literature was found for joining end-plug and tube materials. Representative joining processes are listed in Table 3, and each is briefly described in the following subsections. Note that one of the processing difficulties regarding end-cap joining for a long cladding with thin walls is a limitation in the applied stress that can be employed during joining. In addition, the joining temperature should be low enough to avoid impacting the composite properties by annealing. The strengths of HNS and SA3 SiC fibers are known to degrade under annealing at ~1800°C and ~1900°C, respectively [26]. The effects of irradiation on the joint strengths are reported in the section 4.2.

Table 3. Joining technologies available for SiC

Joining method	Bonding layer	Processing conditions
Solid state diffusion bonding	None or refractory metallic foils such as titanium and molybdenum	~2000°C, >~15 MPa [27, 28] ~1500°C, >~2 MPa [29], (~0.1 MPa [30])
Metallic braze-based	Metallic fillers	~1000°C, low/no pressure [24, 31, 32]
Glass ceramics	Ca-Al-O Si-Al-Mg-O Y-Al-Si-O	~1500°C, no pressure [33, 34]
SiC pre-ceramics precursors	SiC	<~1500°C [35, 36], ~0.01 MPa [35]
Reaction sintering with Si-C and Ti-Si-C systems	Si-C and Ti-Si-C	≤~1500°C [37–39], no pressure [37, 39]
Liquid-phase sintering	SiC powder and sintering additives	~1850°C, ~10 MPa [40, 41]
Selected area CVD/ CVI	SiC	<~1200°C, low pressure [15, 25]

2.5.1 Solid state diffusion bonding

Solid state self-diffusion bonding of SiC to SiC was demonstrated under hot-pressing at ~2000°C under a pressure of >~15 MPa [27, 28]. This joining method allows interface-free joints as a result of thermally activated grain growth across the two bonded substrates. However, the dual requirements of applied stress and very high temperatures during the processing can limit the application of direct bonding to the end-

plug joint. Moreover, direct bonding requires bonding faces with smooth surfaces and decent dimensional control to achieve adequate contact. These technical hurdles suggest another joining option—joining with an interlayer.

Solid state diffusion bonding with an interlayer typically uses a refractory metallic foil such as titanium, molybdenum, and tungsten [29]. The joining method is well established, and the advantage of this joining method is the relatively low joining temperature (~1500°C). The drawback is the need for applied stress of more than a few MPa during the joining. Jung et al. recently overcame this limitation by solid state diffusion bonding using a titanium interlayer and added silicon powder and an applied stress of only ~0.1 MPa [30], which makes this joining method attractive for the end-plug application.

2.5.2 Metallic braze-based joining

Brazing with various metallic filler materials has been widely studied for joining of SiC. For example, fillers of Ni-Cr-Si [31], Ag-Cu-Ti [32], and Al [24] systems were successfully applied to SiC-to-SiC plate joining and/or tube end-cap joining [24]. Brazing typically enables a relatively low processing temperature of ~1000°C and low-pressure or pressureless joining. Since the filler material melts or softens during heating, applying the filler to components with complex geometries is relatively easy.

2.5.3 Glass ceramics joining

Glass ceramics bonding was demonstrated without applying external stress at relatively low temperatures (~1500°C) for Ca-Al-O [34], Si-Al-Mg-O [34], and Y-Al-Si-O [33, 34] systems. The eutectic liquid or softened glass spreads across the joint plane, which enables good contact between the tube and end-cap without applied stress during joining.

2.5.4 Joining using SiC pre-ceramics precursors

This joining method provides a SiC-based joint layer at low processing temperatures (≤~1500°C) [35, 36]) and very low pressures (~0.01 MPa [35]). The common issue with this method is that large-volume shrinkage occurs during the pyrolysis of the precursors, which can cause cracking during the formation of the joint. The addition of SiC powder to the precursor increases the volumetric yield from the precursors and can mitigate issues associated with shrinkage. To form the joint, a bonding agent of a slurry consisting of a SiC forming polymer, a SiC powder, and a solvent may be applied to the joint plane by painting, followed by heating. A limitation of this method is the difficulty of obtaining a dense joint layer.

2.5.5 Reaction sintering with Si-C and Ti-Si-C systems

Reaction sintering or displacement reaction sintering is a method of fabricating ceramics using a powder feedstock; it is also used to join SiC materials. The Si-C [37] and Ti-Si-C [38, 39] systems are used for joining SiC plates. A slurry or green sheet containing the powder feedstock is applied to the bonding plane for joining. The processing temperature is relatively low (≤~1500°C [37, 38]), and pressureless joining has been demonstrated for both reaction systems [37, 39].

2.5.6 Liquid-phase sintering of SiC

Liquid-phase sintering is a method widely used to fabricate dense SiC ceramics using SiC powder and sintering additives (typically oxides such as alumina-yttria) and is also an effective method of joining SiC

materials [40, 41]. The additives form a eutectic liquid during heating, and then the liquid phase promotes the sintering of a SiC powder compact via a solution-precipitation process [42]. The SiC powder mixture with a form of slurry or green tape is applied to the substrate for joining. The reported processing conditions are a maximum temperature of ~1850°C and applied pressure of ~10 MPa for the plate joints. The key development for this joint type is a reduction of the joining pressure and control of the microstructure, especially for the secondary phases, for improved environmental resistance. The use of a nano-size SiC powder helped reduce the amount of sintering additives needed [43].

2.5.7 Selected-area chemical vapor deposition/infiltration

Selected-area CVD or CVI of SiC provides a pure SiC bonding layer, which is expected to be very similar to the CVI matrix. Since this technique is limited to application on only one surface, a hybrid joining technique using SiC pre-ceramic joining followed by CVI SiC was proposed for end-plug applications [25].

2.5.8 Other methods

In the case of an end-plug of NITE SiC/SiC composite cladding, a mechanical joint (screw type) was successfully applied because of the machinability of that composite [19]. A joint interlayer, as discussed in Section 2.5.1, may be applied to achieve adequate gas leak tightness.

3. NONIRRADIATED MATERIAL PROPERTIES

3.1 Physical and Thermal Properties

3.1.1 Density, porosity, and fiber volume fraction

The volume-averaged density of a typical CVI SiC/SiC composite flat specimen ranges from 2.3 to 2.7 g/cm^3 [5]. CVI SiC/SiC is less dense than NITE SiC/SiC [18]. In contrast to the density of fully dense SiC of 3.21 g/cm^3, the density for a CVI SiC/SiC tube without intended CVD SiC coating is reported to be 2.7 g/cm^3 [44]. For NITE SiC/SiC composites, a 95% or higher theoretical density has been reported—about 2.96 g/cm^3 or higher. The porosity of CVI SiC/SiC composite tubes has been reported to be in the range of 8–17% [6, 8, 44–48], which depends on composite design. In the case of CVI SiC/SiC tubes without thick CVD SiC outer/inner layer, the representative porosity is 10–15%. Less than 5% porosity has been reported [49] for NITE SiC/SiC composite tubes. Fiber volume fractions of 30–40% have been generally reported for CVI SiC/SiC full composite tubes, with few exceptions. Table 4 summarizes the physical properties of various types of SiC/SiC tubes.

Table 4. Summary of different SiC/SiC tubes and their physical properties.

Matrix	Fiber	Interphase	Type	Fiber architecture	Density [g/cm^3]	Fiber volume fraction within composite layer [%]	Porosity [%]	Outer diameter [mm]	Wall thickness [mm]	Reference
General Atomics										
CVI	HNS	PyC	n/a	n/a	n/a	30–35	~12	10.63	1.4	[50]
CVI	HNS	150 nm PyC	Duplex with inner CVD SiC	Axial biased (1.5 axial: 1 hoop) Hoop biased, ±45° (1:1)	n/a	n/a	~20	8.8–9.6	1.2–2.1	[6]
CVI	n/a	n/a	Full SiC/SiC duplex	n/a	n/a	35	12.7 8.7	10	1.8	[46]
CVI	HNS	150nm PyC	Full SiC/SiC	±55º from tube axis with axial reinforcement	2.71±0.04	~40	13.8±2.8	9.53	0.78	[44]
CVI	HNS	<250nm PyC	Full SiC/SiC	Axial biased (1.4 axial: 1 hoop)	n/a	36	10	10.2	2.2	[47]
Korea Atomic Energy Research Institute										
CVI	HNS and SA3	200 nm PyC	Triplex	±45º, 55º, 65º	n/a	18–25	10–17% for CVI SiC/SiC layer	9.6–10.1	1.1–1.6	[8]
CEA (French Alternative Energies and Atomic Energy Commission)										
CVI	HNS	100 nm PyC	Full SiC/SiC	±30º along tube axis	n/a	35	~10	9.6	1.7	[48]
CVI	HNS	100 nm PyC	Full SiC/SiC	Three layers ±45° from tube axis	n/a	n/a	10.4–11.1	9.6	1.75	[45]

Matrix	Fiber	Interphase	Type	Fiber architecture	Density [g/cm^3]	Fiber volume fraction within composite layer [%]	Porosity [%]	Outer diameter [mm]	Wall thickness [mm]	Reference
Muroran Institute of Technology										
NITE	n/a	PyC	Full SiC/SiC	±60º from tube axis	n/a	n/a	n/a	10	1	[51]
NITE	n/a	n/a	Full SiC/SiC	n/a	n/a	n/a	<~5%	12	2	[52]

[a] Empty cell information is not currently available.

[b] The new version of Tyranno SA fiber.

[c] "Full" SiC/SiC indicate SiC composite tube without thick inner or outer SiC layer

[d] n/a: information is not available

3.1.2 Thermal expansion

The coefficient of thermal expansion (CTE) of CVI SiC/SiC tubes along tube axial direction was obtained by General Atomics. The result shows similar CTE values among CVI SiC/SiC tube and plate materials (Figure 3). Previous work [5] reported that the instantaneous CTE of CVI SiC/SiC composite plates followed Eq. (1) regardless of the fiber type (HNS or SA3).

$$\alpha\ (10^{-6}/\mathrm{K}) = -0.7765+1.4350\times10^{-2}T-1.2209\times10^{-5}T^2+3.8289\times10^{-9}T^3,\ (293\mathrm{K} < T < 1273\mathrm{K}) \quad (1)$$

where α and *T* indicate CTE and temperature, respectively. This study also confirms that Eq. (1) is applicable to CVI SiC/SiC composite plates neutron irradiated under LWR-relevant temperature and dose conditions (as is discussed later in this report). Therefore, use of Eq. (1) for CVI SiC/SiC tubes is recommended for modeling purposes. For the CTEs of NITE SiC/SiC composites, the data are rare even for a plate specimen. The CTEs of NITE SiC/SiC composites may be assumed to be similar to those of CVI SiC/SiC composites, according to the insignificant effects of oxide phases on the CTEs of monolithic SiC [53].

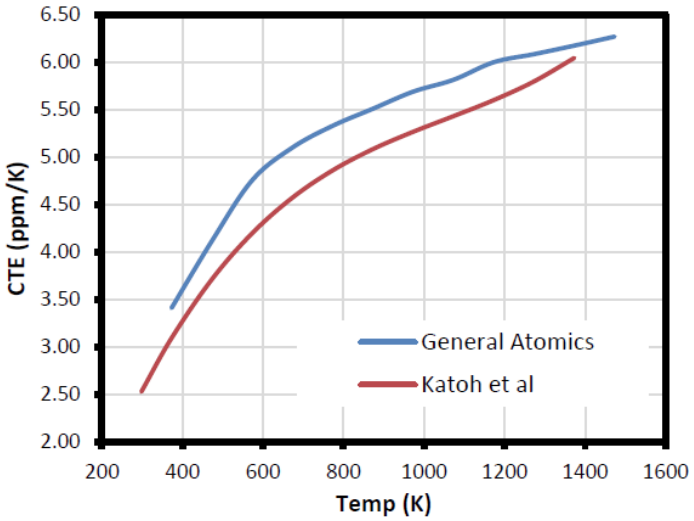

Figure 3 Unirradiated CTE of General Atomics CVI SiC/SiC tubes (unpublished) and CVI SiC/SiC composite flat coupons (Katoh et al. [5]). (Courtesy, General Atomics)

3.1.3 Thermal diffusivity

The thermal diffusivity of the cladding is a key property characterizing the capability for heat transfer from fuel to coolant; thermal conductivity is obtained from the product of thermal diffusivity, density and specific heat capacity. A higher thermal diffusivity results in a lower fuel temperature and smaller through-thickness temperature gradient of the cladding. Therefore, higher thermal diffusivity is usually beneficial for cladding applications.

The thermal diffusivity of SiC/SiC tubes along the wall thickness was evaluated by a laser flash method using a curved square section machined from a SiC/SiC tube [46]. The reported thermal diffusivities are listed in Table 5. Although the measurement method has not yet become a test method standard, the values appeared to be reasonable based on the results from plate specimens [5]. The results showed that

triplex SiC/SiC tubes exhibited higher thermal diffusivity than duplex and full composite tubes because of the higher diffusivity of the monolithic layer compared with the composite layer. There are no data available for the in-plate thermal diffusivity of SiC/SiC tubes because of difficulty of measurement. It is expected that the in-plane diffusivity is higher than the through-thickness diffusivity, according to the results from plate specimens [5]. It is clear that a standard test method for ceramics tubes is needed. Until a standard method is available, thermal diffusivity measurements obtained from plate specimens [5] may be used for modeling purposes.

Table 5. Through-thickness thermal diffusivity of CVI SiC/SiC tubes evaluated using a laser flash method

Material	Room temperature [mm^2/s]	300°C [mm^2/s]	800°C [mm^2/s]	Reference
Duplex SiC/SiC composite with 150 nm PyC coated NHS fiber reinforcement	8~9	4.5~5.5	4~4.5	[6]
Full SiC/SiC composite (no information on fiber type)	2~7	1.25–4.5	1–3.25	[46]
Duplex SiC/SiC composite (no information on fiber type)	8.5–13	5–7.5	3~5	[46]
Triplex SiC/SiC composite with HNS fiber (no interphase information)	~25	~13	No data	[7]

3.1.4 Specific heat

The specific heat of SiC/SiC tubes has not been reported so far. However, the value can be expected to be almost the same as that for SiC/SiC plates. The specific heat of SiC/SiC plates is considered to be the same as that of monolithic SiC (high-purity SiC) because of the negligible effect of the presence of a carbon interphase [5]. The temperature-dependent specific heat of monolithic SiC materials was reported in Snead et al. 2007 [54] (Figure 4).

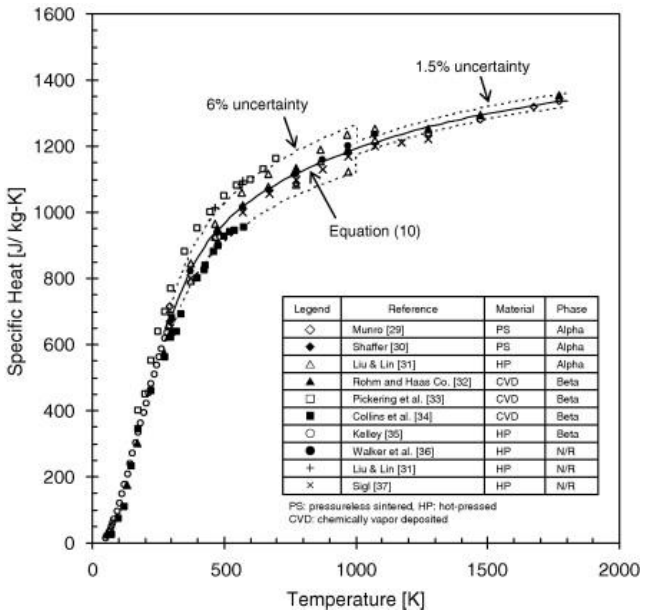

Figure 4. Specific heat of SiC at elevated temperatures [54].

3.1.5 Gas leak tightness

One of the primary functions of the cladding itself is to maintain an impermeable barrier to prevent fission gas release from the fuel into the reactor primary coolant. A criterion of SiC/SiC composite tube failure is a loss of gas tightness. Any increase in the extent of fission gas release from the fuel will be directly proportional to the increase in the radioactivity in the primary coolant and the fission gas (e.g., tritium) release to the environment. Moreover, helium is used as the heat conduction medium between the fuel and the cladding. A loss of hermeticity (an indication of the gas leak tightness) would lead to the release of helium. As a consequence, the heat produced in the fuel could not be efficiently removed and the probability of fuel failure would increase. Therefore, the hermeticity of the SiC-based cladding needs to be assessed.

This section discusses the gas permeability of SiC and the gas leakage rate of a SiC/SiC cladding system. Permeability, an intrinsic physical property of a continuous solid, is expressed as a product of gas solubility and diffusivity. The gas leakage rate is a measure of the effectiveness of the seal of the material or system, as indicated by the flux of gas that passes through the leak.

3.1.5.1 Permeability

Assuming an one dimensional transport, the flux, J, of gas permeating through the sample can be derived from Fick's first law, assuming gas solubility governed by Sieverts' law. It is given by

$$J = \frac{DS(P_i^{1/2} - P_0^{1/2})}{\delta}, \tag{2}$$

where δ is the clad wall thickness of the sample, and P_i and P_o are the gas pressures in the upstream and downstream chambers, respectively. P_o is negligible if the downstream chamber is always under an ultra-high vacuum (~1×10^{-7} torr) during measurement. The product of diffusivity, D, and Sievert's parameter, S, (note that S is usually defined as "solubility" in gas permeation studies) is defined as the permeability, Φ, which can be expressed in the form of

$$\phi = DS = \frac{J\delta}{P_i^{1/2}}, \tag{3}$$

Units used here for D and S are, respectively, m^2/s and *mol* H_2 m^{-3} $MPa^{-1/2}$, giving rise to the unit Φ, *mol* H_2 $m^{-1}s^{-1}MPa^{-1/2}$. Therefore, measurement of the permeation flux will result in the determination of permeability. For most materials, permeability follows the Arrhenius temperature dependence. Thus, it can be expressed as

$$\phi = \phi_0 e^{-\frac{E}{RT}}, \tag{4}$$

where Φ_0 is the permeability constant and E is an apparent activation energy for permeation (essentially the sum of activation energies for dissolution and diffusion). Measurements of the permeability at various temperatures will enable the determination of E and Φ_0.

Various results for the permeation of hydrogen isotopes in SiC have been reported by different authors. An issue in previous efforts has been that most of the work did not show material qualities such as purity and grain size, although different grades of SiC showed significantly different permeabilities. Regardless of the SiC material quality, SiC is considered a good permeation barrier compared to metallic materials. Yamamoto et al. [55] reported the deuterium permeation of CVD SiC fabricated by Rohm and Haas (currently Dow Chemical). The microstructural features of this material exhibited almost full density, a

purity of >99.9995%, an average grain size of ~5 μm, limited grain texture, and the presence of the stacking faults within the grains [56]. The permeation behavior is described by [55] at 600–950°C.

$$\phi = 130e^{-\frac{230kJ}{RT}} mol\, s^{-1}m^{-1}MPa^{-1/2} \quad (5)$$

This result shows that CVD SiC-coated SiC-based cladding is considered gastight in the absence of processing defects and applied strain causing cracks.

3.1.5.2 Gas leakage rate

Based on the requirements for the current Zr cladding system, it is reported that a helium leakage rate should be no greater than 1×10^{-6} mbar ℓ s^{-1} at 17 bar and room temperature for an entire 14 foot fuel rod [25]. Table 6 summarizes the gas leakage rate of CVI and NITE SiC/SiC tubes. Hermetic tubes for both types of materials have been achieved. Although the data positively show hermeticity of the SiC/SiC composite tubes against helium, hydrogen, and deuterium even at 300°C, a probabilistic leaking rate is missing in the current database. Since a single micro-crack penetrating wall of cladding can cause leaking, it will be necessary to statistically assess gas leak tightness of SiC/SiC cladding and probability of such defect in cladding.

Table 6. Gas leakage rate for SiC/SiC tubes

Material	Specimen geometry [mm]	Test condition	Gas leak rate	Reference
CVI SiC/SiC tube with SiC end-plug	ID ~7.5 Wall thickness 1.2-2.1	Gas: He ΔP =0.1MPa @ room temperature	<1.01×10^{-13} Pa m^3/s	[6]
		Gas: He ΔP =0.1 MPa @ 300ºC (after 1000ºC thermal cycle and 16.8 MPa applied gas pressure)	4.1×10^{-10} Pa m^3/s	
CVI SiC/SiC tube coated with CrN or TiN and open ends	Length 16 ID 7.1 Wall thickness 1.4	Gas: He and D_2 ΔP ≤ ~0.1 MPa @ room temperature	<1.01×10^{-13} Pa m^3/s for both He and D_2	[57]
NITE SiC/SiC tube with open ends	Length 200 ID 10 Wall thickness 1 (uniform heating length, 30 mm)	Gas: He and H_2 ΔP < 0.01MPa	He <2×10^{-12} Pa m^3/s up to 400ºC H_2 <1×10^{-8} Pa m^3/s up to 400°C	[51]

3.2 Mechanical Properties

Properties related to mechanical failure include the stresses for the first major matrix cracking, the first penetrating crack formation, and ultimate failure. Statistical factors for these properties are insufficiently understood for nuclear-grade SiC/SiC composite tubes. The statistical factors include both the governing statistic laws and statistical parameters such as Weibull parameters. These are especially important at the extremes of the failure distribution. Part of the focus of this section is the mechanical properties

dependence on the fiber reinforcement angle. This dependence has been reported in both filament-wound and 2D braided CVI SiC/SiC tubes, although a detailed analysis was not provided [11].

3.2.1 Elastic properties

The typical in-plane Young's modulus for nuclear-grade CVI SiC/SiC composite planar specimens has been reported to be in the range of 200–280 GPa [5]. Shear modulus value ranging from 80–120 GPa have been reported for flat specimens [5].

Compared with planar specimens, fewer studies have been conducted for tubular full SiC/SiC composites, and Young's moduli, mostly from tensile tests, are available in the literature. The reported Young's moduli for axial tensile tests mostly lie in the range of 173–248 GPa [6, 44, 45, 47, 48], except for relatively low value of 129 GPa obtained in [6]. For hoop tensile tests, limited studies [6, 47, 48] have reported the value of Young's modulus to be 158–213 GPa for full SiC/SiC composite tubes. One study has reported the Young's modulus under compression: 251 GPa [45].

For tube specimens, the coefficient of variance (C.V.) for Young's modulus has been reported to be mainly in the range of 7–20% [6, 44, 45, 48]. A round-robin study showed a significant variation in C.V. across the laboratories, indicating a strong dependence on the material, operator, and test equipment of the spread in the modulus data [44].

Nozawa et al. [58] report the in-plane Poisson's ratios for plate specimens oriented at different angles from the direction of loading. The reported data show that when the fiber orientation with loading was changed from 0º/90º to ±45º, the Poisson's ratio increased from ~0.13 to ~0.25 for plain-weave CVI and NITE SiC/SiC composites under tensile as well as compressive tests. Poisson's ratio of 0.12 in the axial direction was reported for CVI SiC/SiC tube [47]. Figure 5 shows the Young's modulus determined from various studies of tubes. The linear fit line indicates a moderate effect of fiber winding angle on the axial Young's modulus of SiC/SiC tubes.

Although elastic properties of SiC/SiC tubes have been reported as described above, no complete evaluation of elastic properties of SiC/SiC tubes considering material anisotropy has been conducted. In the case that the SiC/SiC composite tube is considered as an orthotropic material, the elastic behavior can be described using nine independent elastic constants: E_r, E_θ, E_y, $\nu_{r\theta}$, ν_{ry}, $\nu_{\theta y}$, $G_{r\theta}$, G_{ry} and $G_{\theta y}$, where E represents Young's modulus, ν represents Poisson's ratio and G represents shear modulus; see Figure 6. The subscripts r, θ and y represent the radial, circumferential and axial directions respectively. To obtain all of the elastic properties from a single test method, we utilized resonant ultrasound spectroscopy to evaluate elastic properties of SiC tube specimens, which has successfully been applied to monolithic tube [59]. Figure 6 presents a preliminary result of resonant ultrasound spectroscopy of SiC/SiC composite tube. The material is CVI SiC/SiC composite fabricated by General Atomics [44]. The current focus of this work is validation of the analysis result based on Young's modulus of the specimens obtained from tube tensile and hoop tests. Development of resonant ultrasound spectroscopy technique for SiC/SiC composite tube is important because there have not been other methods proposed for full evaluation of anisotropy of the elastic properties. The elastic properties in Figure 6 may be used as input parameters for the modelling of CVI SiC/SiC composite cladding. Table 7 summarizes the tensile and hoop mechanical behavior of the SiC/SiC tube specimens.

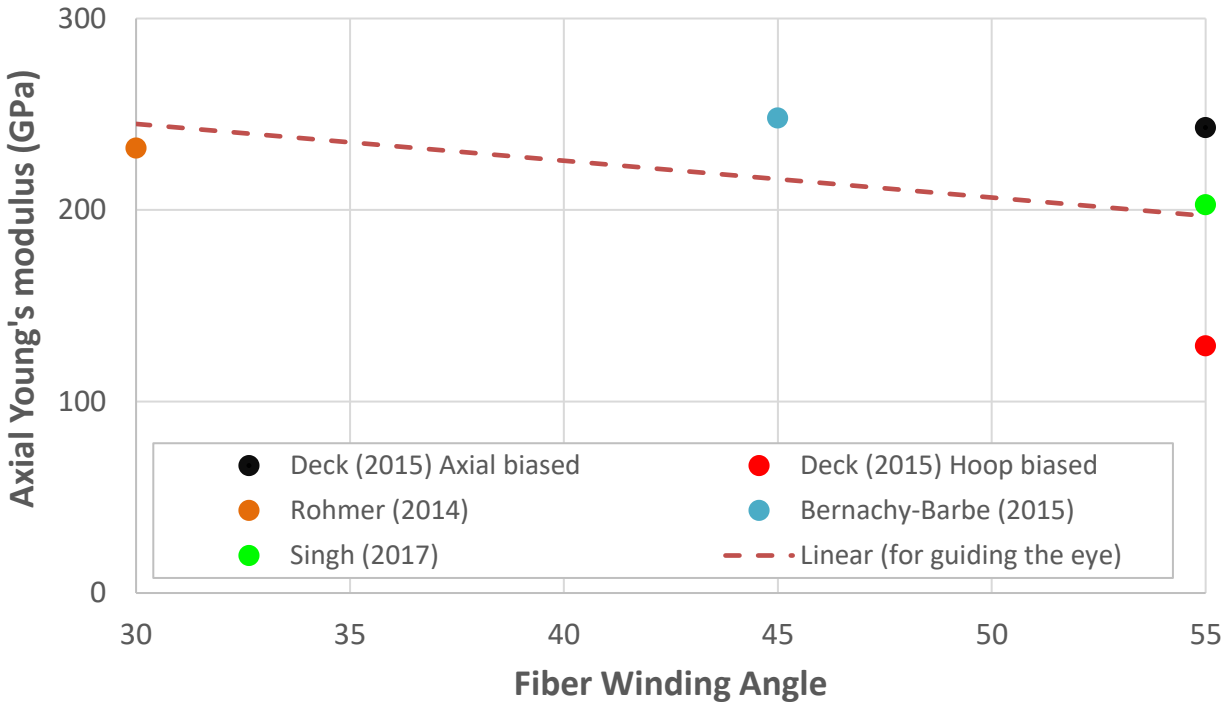

Figure 5. Axial Young's moduli determined from several studies for CVI SiC/SiC tubes.

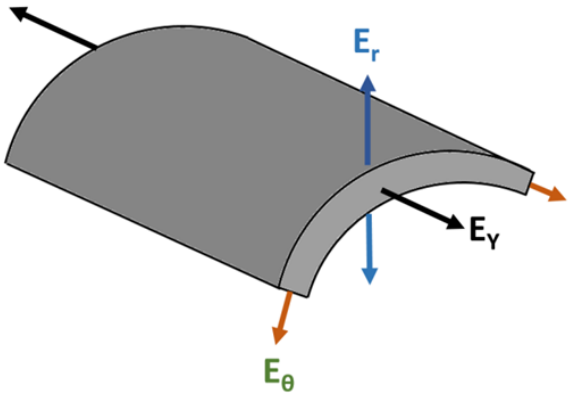

	Mean	Standard deviation
E_r (GPa)	79.9	8.4
E_θ (GPa)	248.8	12.4
E_Y (GPa)	263.9	15.0
$\nu_{r\theta}$	0.191	0.042
ν_{rY}	0.204	0.042
$\nu_{\theta Y}$	0.170	0.035
$G_{r\theta}$ (GPa)	70.5	6.3
G_{rY} (GPa)	85.7	9.8
$G_{\theta Y}$ (GPa)	109.5	6.4

Figure 6 Elastic properties of SiC/SiC composite tube determined by resonant ultrasound spectroscopy. The material information is shown in [44].

Table 7. Compilation of mechanical properties of SiC/SiC composite determined from tests on tube specimens

Material	Loading (Test method)	Young's modulus (GPa)	PLS (MPa)	UTS (MPa)	Strain at PLS (%)	Strain at UTS (%)	Shear strength (MPa)	Number of test	Fiber architecture/ porosity/fiber volume fraction	Ref.
CVI, HNLS 100 nm PyC	Uniaxial tension (Monotonic axial tensile test)	248 (14)	~100	269	~1			3	±45°, inner layer filament wound, outer layers 2×2 braids/10.4–11.1%	[45]
	Uniaxial compression (Monotonic axial compression test)	251 (15)	~130	385				3		
	Hoop tension (Internal pressurization)			303				3		
	Equibiaxial (tension, internal pressurization)			297				2		
	Torsion						286			
Full SiC/SiC axial biased[1]	Hoop tension (C-ring)			209 (24)					±~50-~60°/~20%/-	[6]
Full SiC/SiC hoop biased[2]	Hoop tension (C-ring)			331 (74)						
Full SiC/SiC, axial biased[1]	Uniaxial tension (Monotonic axial tensile test)	243 (19)		236 (35)						
Full SiC/SiC hoop biased[2]	Uniaxial tension (Monotonic axial tensile test)	129 (14)		93 (14)						
Duplex: Monolith (inside) and SiC/SiC	Hoop tension (C-ring)			174 (28), [3]m=7.0						
Full SiC/SiC	Hoop tension (C-ring)			209 (24), m=7.9						
Duplex: Monolith (outside) and SiC/SiC	Hoop tension (C-ring)			311 (59), m=4.6						
Full SiC/SiC	Hoop tension (C-ring)			304 (14), m=12.1						
Duplex: Monolith (inside) and SiC/SiC	Hoop tension (expanding plug)	278 (20)	[4]OD: 92 (6), [5]ID: 140 (7)	OD: 152 (8) ID: 231 (9)						
Duplex: Monolith (outside) and SiC/SiC	Hoop tension (expanding plug)	288 (13)	OD: 129 (10) ID: 158 (12)	OD: 271 (2), ID: 332 (3)						

Material	Loading (Test method)	Young's modulus (GPa)	PLS (MPa)	UTS (MPa)	Strain at PLS (%)	Strain at UTS (%)	Shear strength (MPa)	Number of test	Fiber architecture/ porosity/fiber volume fraction	Ref.
Triplex: CVI SiC/SiC at middle, monolith outside and inside, 200 nm PyC (SA3, HNLS)	Hoop tension (internal pressurization)			282.4 (44.3); m=11.05					See Section 3.2.2, ±45º, ±55º, ±65º	[8]
CVI SiC/SiC, HNLS	Axial tension (monotonic axial tensile test)	232.2 (17.1)	82.75 (12.76)	462.7 (37.3)	0.034 (0.007)	0.685 (0.087)		4	±30º/ - /35%	[48]
CVI SiC/SiC, HNLS	Hoop tension (internal pressurization)	157.5 (27.6)	35.5 (6.36)	63 (0.7)	0.032 (0.015)	1.51 (0.014)		2		
CVI SiC/SiC, HNLS, 150nm PyC	Axial tension (monotonic axial tensile test)	202.7 (40.3)	92.6 (9.0), log mean: 4.52, log standard deviation: 0.096	236.8 (29.6), m=10.1	0.057 (0.007)	0.53 (0.1)		43	±55º with axial reinforcement/14%/51%	[44]
CVI SiC/SiC, HNLS, <250nm PyC	Uniaxial tension (Monotonic axial tensile test)	173 (19)	104 (7)	245 (8)	0.0634 (0.01)	0.6402 (0.04)		3	hoop to axial direction: 1:1.4, 10%/36%	[47]
	Hoop tension (Elastomeric Insert)	213 (37)	ID: 147 (8) OD: 110 (8)	ID: 449 (13) OD: 336 (14)	0.0540 (0.0071)	0.8165 (0.0210)		5		
	Hoop tension (internal pressurization)	201 (23)	ID: 126 (14) OD: 93 (11)	ID: 380 (27) OD: 281 (21)	0.0552 (0.0071)	0.7627 (0.1076)		10		
	Torsion	101 (5)			0.1272 (0.0087)	0.6606 (0.0864)	PLS: 119 (14) Ultimate shear: 229 (3)	2		

Values in brackets are one standard deviation from the mean.
1 Fiber reinforcement ratio (hoop: axial) 1: 1.5
2 Fiber reinforcement ratio (hoop: axial) 1.3: 1
3 Weibull modulus
4: Outer diameter
5: Inner diameter

3.2.2 Proportional limit stress

For flat specimens, the proportional limit stress (PLS) has most frequently been reported in the 90–120 MPa range under monotonic tension along a direction of fiber reinforcement [5]. For tube specimens, axial PLS has been generally reported between 80 and 100 MPa [44, 45, 47, 48]. In the hoop direction, the typical value is ~100 MPa in case there is no thick monolithic SiC inner or outer layer. Bernachy-Barbe et al. [45] report axial PLS of about 130 MPa under compression, which is slightly greater than the reported PLS under tension (about 100 MPa). Most studies report a standard deviation of 10 MPa or less. Note that the PLS presented here is typically determined by the 0.001% strain offset method or onset of an energy or hit count of acoustic emission. Fiber architecture greatly influences the PLS. Nozawa et al. [58] has systematically shown the effect of fiber orientation on mechanical properties in flat specimens; PLS decreases by over 25% when the fiber orientation is changed from 0°/90° to ±45°. Tests conducted by Rohmer et al. [48] on tube specimens with ±30° fiber orientation led to a PLS of 36 MPa in the hoop direction and 83 MPa in the axial direction.

3.2.3 Ultimate tensile strength

An in-plane UTS of 250–350 MPa has been generally reported for flat specimens [5]. For tube specimens, UTS has been measured as being in the range of 230–270 MPa in the axial direction and 200–340 MPa in the hoop direction in most studies [6, 8, 44, 45, 47, 48]. The strength values reported toward the higher end of this range are for specimens having a fiber fraction biased in the hoop direction [6]. The typical C.V. for UTS for tube specimens ranged between 10 and 20 %, although C.V.s outside this range have been also reported.

There is a significant effect of fiber orientation on the UTS. Nozawa et al. [58] measured a decrease in UTS (failure stress) of about 35% upon changing the fiber orientation by 45° in flat specimens. Rohmer et al. reported a significantly smaller hoop strength (63 MPa) than the axial strength (463 MPa) for tube specimens with a ±30° fiber orientation with regard to the tube axis. Kim et al. [8] tested triplex SiC tube specimens and showed an increase in the hoop strength by over 15% after an increase in the fiber orientation from ±45° to ±65° for SiC triplex tubes. The hoop strength of the specimens ranged from 235 to 338 MPa. In the Kim et al. study, tubes with Tyranno SA3 fibers exhibited greater strength than tubes with HNS fibers; the study also shows that the fiber winding method influences the strength significantly.

Figure 7 and Figure 8 show the axial and hoop UTS determined from various studies involving SiC/SiC tube specimens. The steep slope of the linear fit indicates a significant effect of the fiber reinforcement angle on UTS.

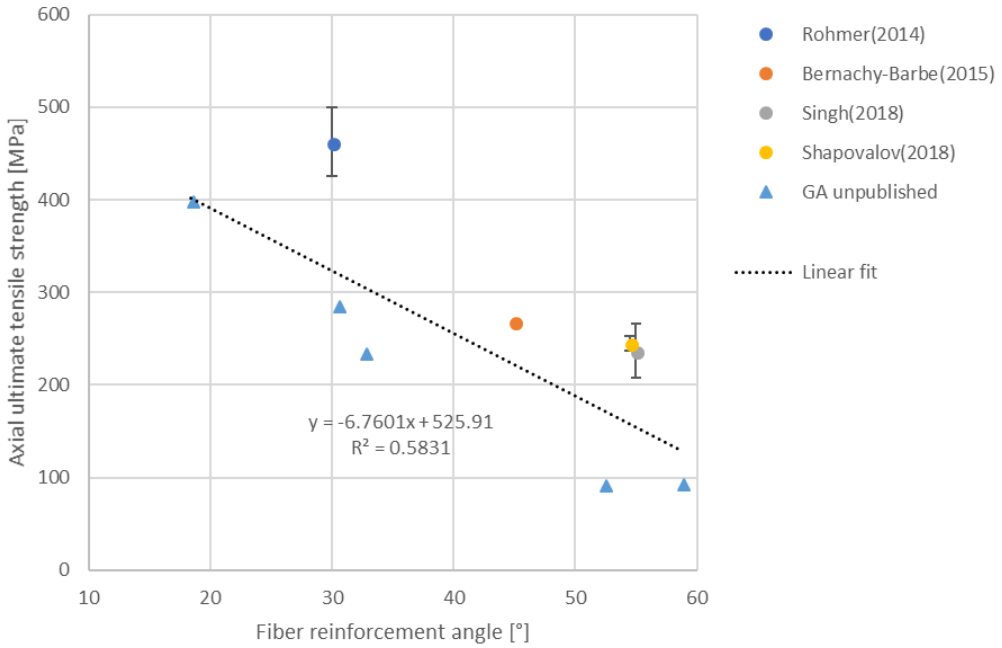

Figure 7. Axial UTS of CVI SiC/SiC tubes. For the part of data, the ratios of fiber reinforcement between axial and hoop directions are converted to equivalent fiber reinforcement angles.

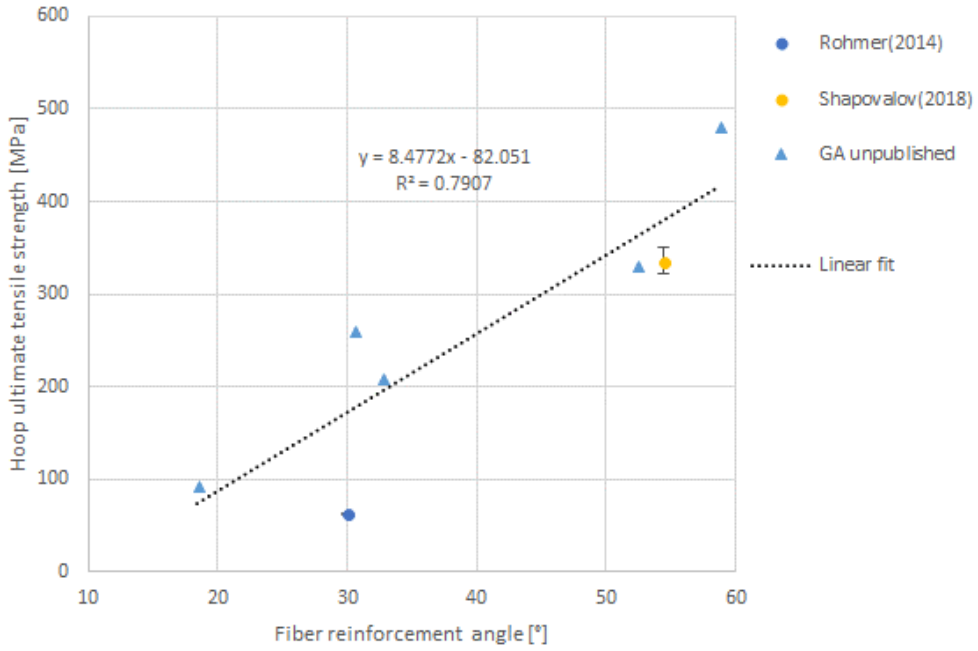

Figure 8. Hoop UTS of CVI SiC/SiC tubes. For the part of data, the ratios of fiber reinforcement between axial and hoop directions are converted to equivalent fiber reinforcement angles.

3.2.4 Strain at proportional limit strength and ultimate tensile strength

The strain at PLS has been measured to be in the range of 0.03–0.06% for studies involving tubes, and strain at UTS has been reported to range from 0.5 to 0.85% [44, 45, 47, 48]. The C.V.s for strains at PLS and UTS range from 10 to 20% for most studies on tubes.

3.2.5 Statistics of mechanical properties

Statistics of mechanical properties are an essential data for prediction of failure probability of SiC based fuel cladding under a service environment. However, that information is currently limited maybe due to limited number of specimen available for testing. Recently, Singh et al. conducted interlaboratory round robin study on tensile strength of CVI SiC/SiC composite tubes reinforced with HNS fiber, fabricated by General Atomics [44]. In that study, 47 tubular specimens were tested at room temperature according to ASTM C1773 [60]. It was found that the distribution of PLS was best described with a lognormal distribution with the log-mean and log-standard deviation of 4.52 and 0.096, while a two parameter Weibull distribution with shape parameter of 10.13 and scale parameter of 249.08 were good descriptors of the distribution of UTS. The analysis results are shown in Figure 9.

It is noted that actual SiC/SiC composite cladding will experience multi-axial loading [61] so that statistical data from tensile tests may not be simply applied to the modeling. However, the data provided by Singh et al. [44] is one of the best data for the modelling purposes currently due to limited studies on statistics of mechanical properties of SiC/SiC tube. Additional statistical evaluation of tube under multi-axial loading conditions is required for future study.

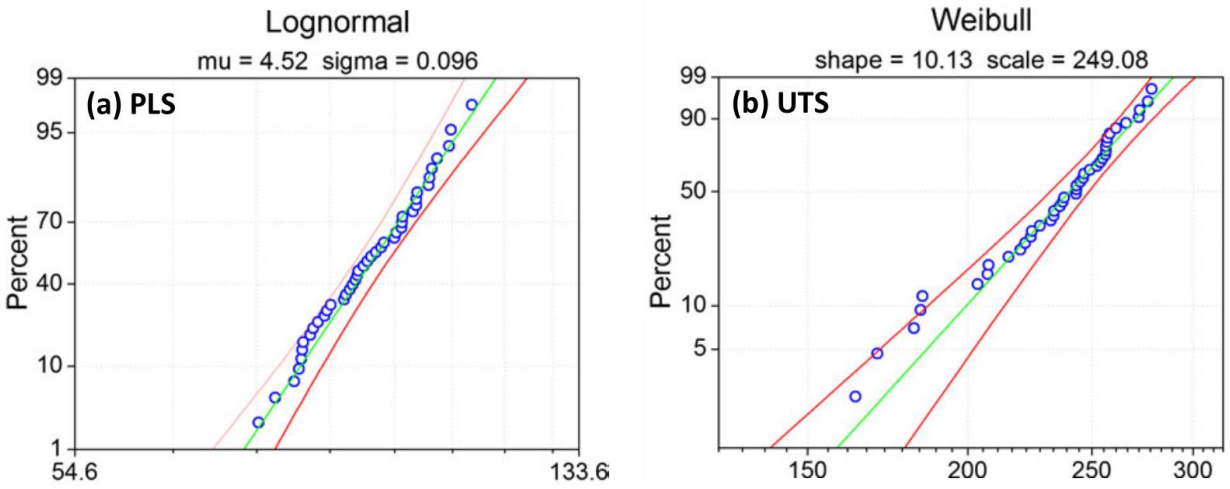

Figure 9 Fit of (a) PLS and (b) UTS data to lognormal and Weibull distribution functions, respectively, with 95% confidence bound lines in red (units: MPa) [44].

3.2.6 Thermal creep

In general, the thermal creep rates for SiC based materials are very low at below ~1000°C. Therefore, for LWR normal operation temperatures, thermal creep is completely negligible for a thermo mechanical modeling of SiC cladding. Recently, it was demonstrated that superior creep rupture properties of CVI

SiC/SiC composite plates reinforced with SA3 fibers at 1000°C in vacuum under tensile stresses of both below and above the PLS [62].

3.3 Corrosion, Oxidation and Fuel Compatibility

3.3.1 Hydrothermal corrosion

SiC recession as a result of corrosion in high-temperature water leads to (1) cladding thickness losses that could in turn result in increased loading on the structure and (2) deposition of unwelcome corrosion products in the primary water circuit. Therefore, it is essential to quantify the rate of SiC recession, along with its dependence on environmental conditions such as pH, oxygen potential, electrochemical potential, solutes in the aqueous systems, and radiolysis. This section discusses the corrosion behavior of SiC materials and candidate EBC materials in simulated reactor coolant without considering irradiation effects such as displacement damage and radiolysis.

3.3.1.1 Corrosion of SiC matrix

In the case of a cladding design without a non-SiC EBC, the SiC matrix is expected to be the first barrier against the coolant water, and no fiber and carbon interphase are expected to be exposed. Figure 10 summarizes the hydrothermal corrosion behavior of monolithic high-purity CVD SiC. It corresponds to the matrix of a CVI SiC/SiC composite in a simulated reactor coolant environment, including pressurized water reactor (PWR), boiling water reactor (BWR) hydrogen water chemistry (HWC), and BWR normal water chemistry (NWC), all neglecting irradiation [63, 64]. Figure 10 clearly shows that different water chemistries lead to different corrosion behaviors. The previous corrosion study highlighted that the dissolved oxygen activity in water greatly increased SiC recession. Not only the water chemistry, but also material qualities such as grain size and grain texture, likely affect the corrosion resistance, since preferential attack at the grain boundary has been reported [63, 64]. In fuel cladding applications, depending on the in-pile recession kinetics of SiC and the thickness of the matrix on the surface, a loss of cladding thickness can potentially expose the fiber-matrix interphase. This exposure can lead to damage to the fiber and/or interphase and consequently degrade the composite's mechanical properties.

The kinetics of SiC recession under hot water is governed by a surface oxidation reaction (silica formation), because once silica forms on SiC under hydrothermal conditions, it readily dissolves in water. Therefore, it is also important to consider that the silica concentration in the reactor coolant can reach its solubility limit, and then the silica will deposit in the relatively cold regions of the coolant loop [63]. It is doubtful that significant amounts of deposited silica in the reactor core can be allowed during operation.

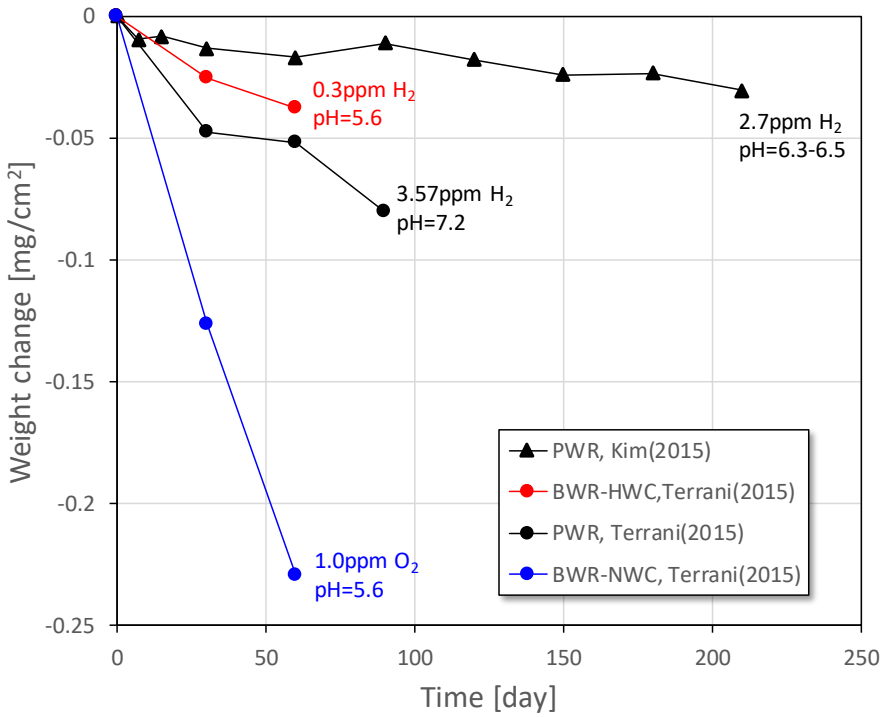

Figure 10. Mass change in CVD SiC after exposure to simulated reactor water loops [63, 64]. The temperature and pressure ranged from 290 to 360°C and 7–20 MPa, respectively, depending on the water chemistry.

For NITE SiC/SiC composites, a systematic investigation of the hydrothermal corrosion behavior of the matrix has not been reported. However, the corrosion behavior has been investigated for monolithic SiC ceramics. Their microstructure was found to be similar to that of the NITE matrix: a relatively small grain size (submicron to a few microns) and the presence of oxide secondary phases along the grain boundaries (as a thin film a few nm in width) and at grain pockets. These monolithic SiC ceramics are referred to as "NITE ceramics" in this paper for convenience. Parish et al. report the recession of NITE SiC ceramics with three different additive systems under the simulated PWR, BWR-HWC, and BWR-NWC coolant environments without irradiation, as shown in Figure 11 [20]. The recession rates of NITE SiC ceramics were more than one order higher than those of CVD SiC specimens; the poor corrosion resistance was attributed to the secondary phases preferentially attacked under hydrothermal conditions. This work also demonstrated that corrosion properties can be improved by controlling secondary phases. At the time of the current report, hydrothermal corrosion–resistant NITE SiC/SiC composites have not yet been demonstrated. An EBC on the clad surface may be an option for NITE SiC/SiC cladding.

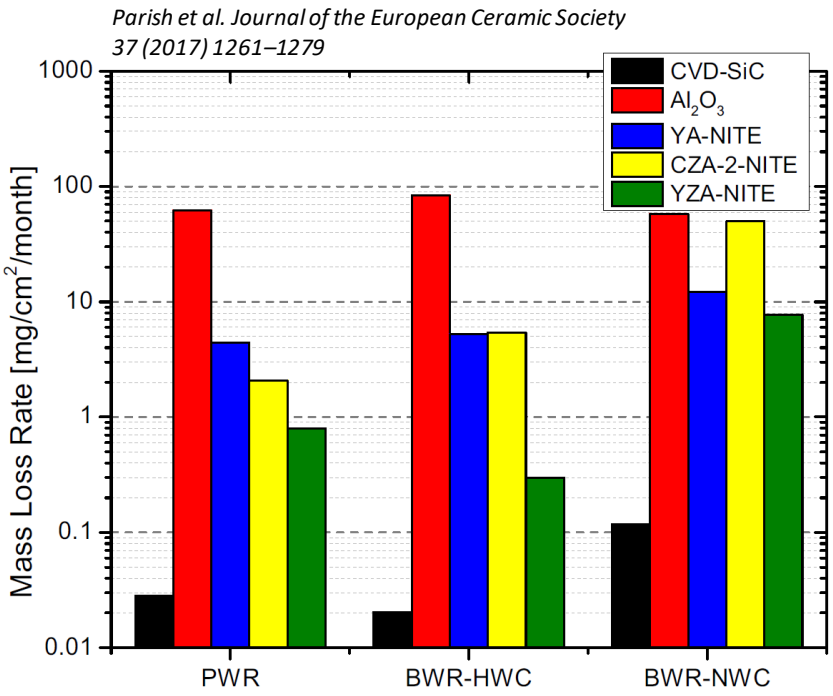

Figure 11. Linear mass loss rate for NITE SiC with various sintering additives, CVD-SiC, and polycrystalline alumina [20]. The corrosion test was conducted for up to 3 months for CVD SiC, 2 months for YA-NITE, and 5 weeks for the other materials. YA-NITE, CZA-2-NITE, and YZA-NITE are NITE ceramics fabricated with sintering additives of Y_2O_3-Al_2O_3, CeO_2-ZrO_2-Al_2O_3, and Y_2O_3-ZrO_2-Al_2O_3 systems, respectively.

3.3.1.2 Corrosion of SiC joint

Hydrothermal corrosion of the end-plug joint is also considered a feasibility issue. The allowable recession rate may depend on the joint geometry; a larger bonding area provides more allowance for recession. Koyanagi et al. report the hydrothermal corrosion behavior of various SiC-to-SiC plate joints under simulated reactor coolant environments for 5 weeks [39]. The tested joints include a molybdenum diffusion bond, a titanium diffusion bond, a Ti-Si-C reaction sintered bond, and a SiC nanopowder sintered bond. Under a reducing activity environment (PWR and BWR-HWC), only the molybdenum diffusion bond showed poor corrosion resistance (Figure 12a). However, under a BWR-NWC oxidizing activity environment, all of the joints except the SiC nanopowder sintered joint experienced significant recession. The sintered SiC joint exhibited only a 5 μm recession relative to the CVD SiC substrate following corrosion testing for 5 weeks (Figure 12b). Another promising joint was a selected-area CVD or CVI SiC joint that forms a high-purity SiC bonding layer.

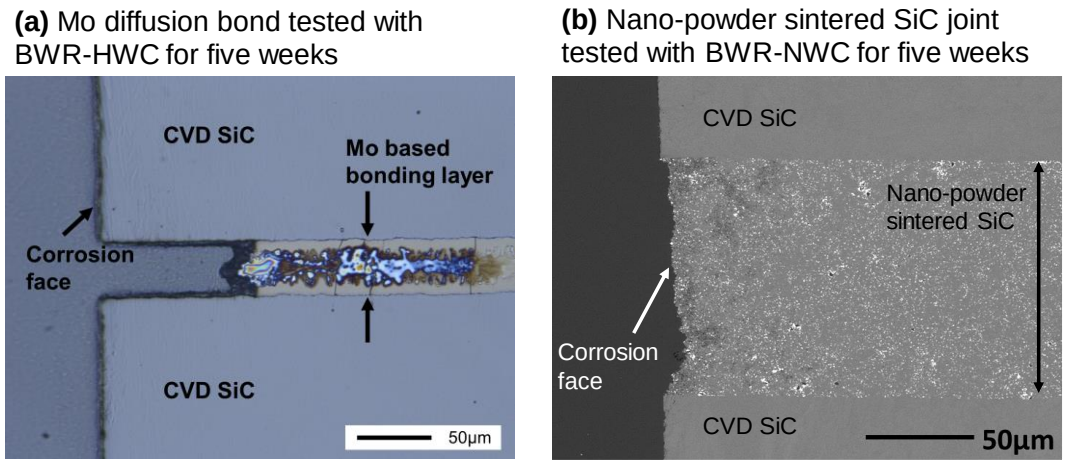

Figure 12. Cross-sectional observation of SiC joints after autoclave immersion: (a) molybdenum diffusion bond tested with BWR-HWC for 5 weeks and (b) nanopowder sintered SiC joint tested with BWR-NWC for 5 weeks [39].

3.3.1.3 Corrosion of coating

An EBC on the outer surface of the cladding will be required if SiC composites undergo unacceptable recession in the coolant. Several types of corrosion-resistant EBCs are under development for Zr-based claddings [21]. The corrosion-resistant coating materials applicable for SiC include chromium-based (chromium and CrN [65–68]), and titanium-based (TiN/Ti layer [69, 70] and TiAlN [71]). The reported corrosion resistance of each of these coatings is summarized in Table 8. All of the coating materials exhibited weight gain and superior performance to a reference Zr-based alloy under hydrothermal environments. Although the coating is not on SiC substrate, the information in Table 8 shows these coating materials are potentially useful for SiC cladding systems.

Table 8. Hydrothermal corrosion resistance of coated materials. The coated zirconium-based alloy was tested unless otherwise indicated

Material	Coating method	Corrosion environment	Corrosion test results	Reference
Bulk Cr	Not applicable	–360°C/18.9 MPa – Static autoclave	Weight gain of 3.2 mg/dm^2 after 15 days	[65]
Cr coating on Zr	Physical vapor deposition	–360°C –Simulated PWR primary water –Autoclave	Weight gain of ~5 mg/dm^2 after 60 days	[66, 67]
CrN coating on Zr	Physical vapor deposition	–300°C/pH$_{25°C}$:10.5 –LiOH addition –Static autoclave	Better corrosion resistance compared with Zr-4 after 30 days	[71]
CrN coating on Zr	Physical vapor deposition	–In-pile test –PWR condition at 320°C –150 days –Fast neutron fluence: 1.8×10^{24} n/m^2	Insignificant change in the coating thickness by irradiation Local oxidation of the substrate	[68]

A limited data is also available for hydrothermal corrosion of those coating candidates on CVD SiC substrate [72]. The corrosion test was conducted in 288 °C water with 2 wppm dissolved oxygen in a

constantly-refreshing autoclave without irradiation. Evaluation of those coating exposure simultaneous neutron irradiation and simulated pressurized water reactor coolant in MIT reactor is ongoing, which will provide insight of suitable coating system for LWR applications.

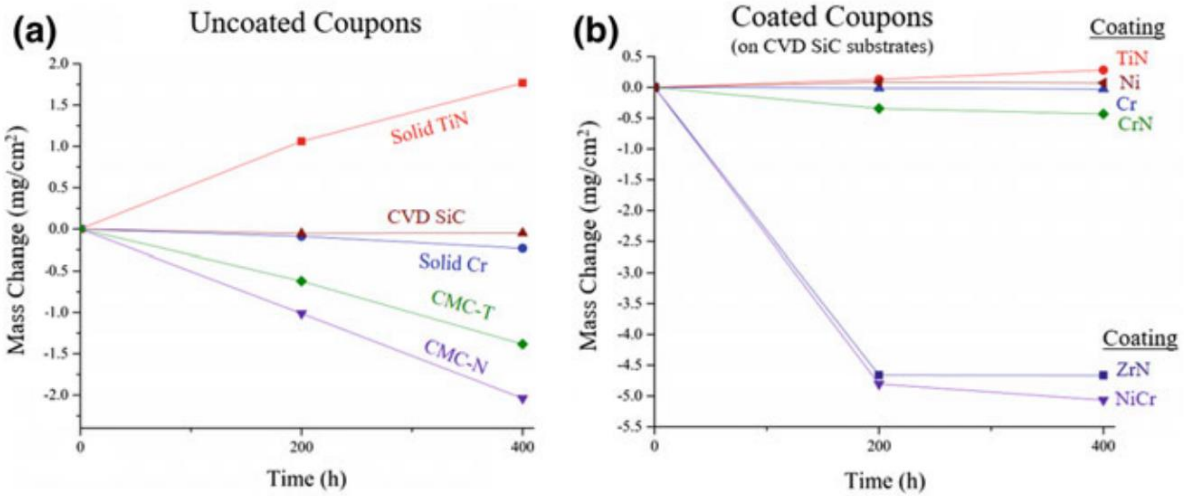

Figure 13 Mass change of (a) bulk coating candidates and (b) coated SiC specimens. Corrosion test was conducted in 288 °C water with 2 wppm dissolved oxygen in a constantly-refreshing autoclave to simulate BWR–NWC. The graph reprinted from [72].

3.3.2 Fuel-clad chemical and mechanical interaction

The chemical compatibility of SiC cladding with fuels under normal operation and accident conditions is of great importance. The cladding inner surface comes in contact with the fuel, depending on the initial gap and the swelling behavior. Fission product transportation and interactions with SiC, SiC/SiC composites, the composite constituents, and internal interfaces also need to be understood for all gaseous and metallic fission products and their daughters. The fission products of primary interest include noble metals and tritium.

For a SiC/$UO_{2\pm x}$ system, Braun et al. experimentally investigated the reactivity and concluded that (1) limited chemical reaction occurs up to 1241°C and (2) a liquid phase forms between 1577 and 1677°C in the open and closed SiC/$UO_{2\pm x}$ system [73]. Silva et al. reported that the microstructure of high-purity SiC, such as the grain boundary structure, affected the chemical reaction between SiC and UO_2 at 1500°C [74]. The reaction temperatures reported are much higher than the temperature of the cladding under normal operation.

Gerczak et al. discussed the potential reactions between SiC and various fission products, including fission gases, metallic precipitates, and oxide phases [75]. According to previous studies (typically a thin foil diffusion couple study), they concluded that SiC is susceptible to reaction with various fission product elements in the fuel system; however, the temperature of the SiC clad is not sufficient to promote significant interactions due to the reaction kinetics.

Study on the fuel-clad mechanical interaction is significantly limited and was conducted only under simulated condition [50].

3.3.3 Steam oxidation

The oxidation resistance of CVD SiC, the expected first barrier against steam attack in CVI SiC/SiC tubes, is discussed in this section. Oxidation of SiC under a high-temperature steam environment is expressed by paralinear kinetics: parabolic oxidation forming silica on SiC and linear volatilization of the silica [2]. The parameters affecting the steam oxidation behavior include temperature, exposure time, steam flow rate, and steam pressure. The parabolic oxidation constants for SiC in flowing 0.1 MPa steam are reportedly ~3 orders of magnitude smaller than those for Zircaloy-4 in a temperature range 1200-1500 °C [2]. Figure 14 shows the steam oxidation behavior of CVD SiC based on the experimental results (for SiC). An outstanding low recession rate for CVD SiC compared with Zircaloy-4 was reported. The results shown in Figure 14 are consistent with the results from different steam oxidation studies using high-purity CVD SiC [76], a CVD-coated CVI SiC/SiC composite [77], and sintered SiC (SE type Hexoloy) [78] under different steam oxidation conditions.

Monolithic SiC fabricated via liquid-phase sintering of SiC nanopowder and oxide additives, a similar material with a matrix of NITE SiC/SiC composite, also showed significant steam oxidation resistance compared with Zircaloy-4 at up to 1200°C [79], indicating NITE SiC/SiC cladding improves the safety of the cladding system in the case of an accident.

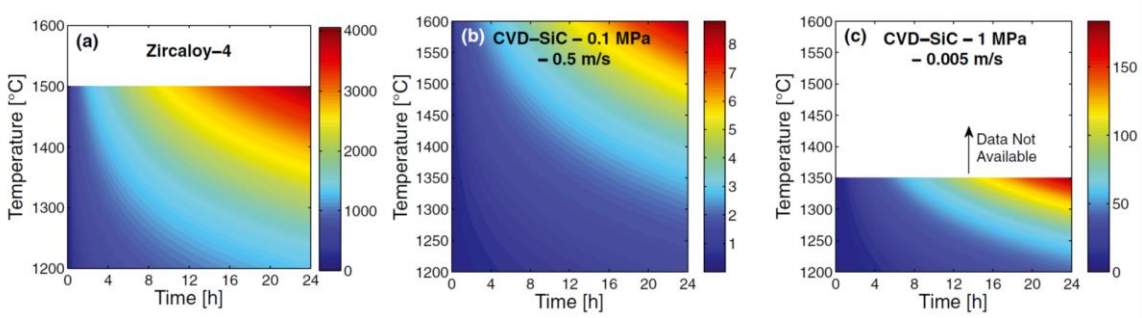

Figure 14. Thickness consumed (in μm) during steam oxidation: (a) Zircaloy-4 and (b, c) CVD SiC. (Reprinted from Terrani 2014 [2])

4. IRRADIATED MATERIAL PROPERTIES

4.1 Physical and Thermal Properties

4.1.1 Swelling

The density of SiC/SiC cladding changes as a result of irradiation-induced swelling. Accurate data for temperature- and dose-dependent swelling of SiC/SiC materials are essential for multi-physics modeling of the cladding. A swelling gradient across the clad thickness direction, resulting from the through-thickness temperature gradient, is a great concern because it builds significant stress within the cladding [61]. Swelling of SiC/SiC plates has been evaluated for various irradiation conditions as summarized in [5], and those date are applicable to the tube specimens. The swelling of both HNS fiber reinforced CVI SiC/SiC composite plate along in-plane direction and CVD SiC is expressed by Eq. (6), based on recent swelling evaluation by an accurate method of both dimensional change and irradiation temperature [80].

$$S = S_S\left[1 - exp(1 - \frac{\gamma}{\gamma_C})\right]^{2/3} \qquad (6)$$

$$\gamma_C = -0.57533 + 3.3342 \times 10^{-3}T - 5.3970 \times 10^{-6}T^2 + 2.9754 \times 10^{-9}T^3 \qquad (7)$$

$$S_S = 5.8366 \times 10^{-2} - 1.0089 \times 10^{-4}T + 6.9368 \times 10^{-8}T^2 - 1.8152 \times 10^{-11}T^3 \quad (8)$$

S, *γ*, and *T* denote swelling, displacement damage in dpa for SiC, and irradiation temperature, respectively. The obtained irradiation-dose and -temperature dependences of swelling are shown in Figure 15. Equation (6) is also applicable to CVI SiC/SiC composites with SA3 fibers based on similar swelling to HNS CVI SiC/SiC composites [81]. Applicability of Eq. 6 to swelling of SiC composite tubes will be demonstrated though post-irradiation examination that is currently ongoing [82].

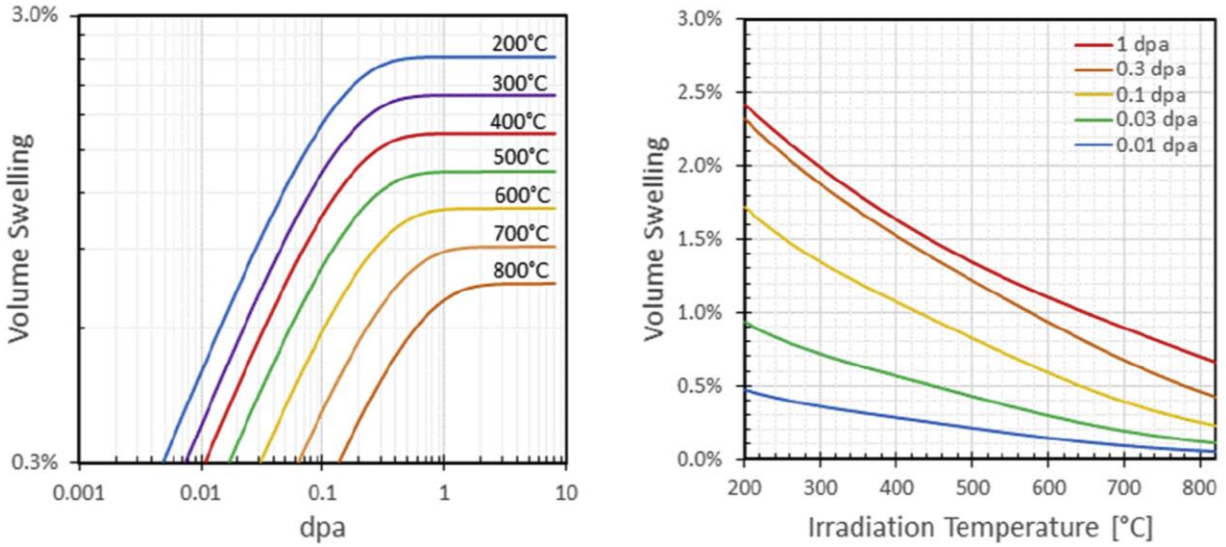

Figure 15. Irradiation dose and temperature dependence of swelling of CVD SiC and CVI SiC/SiC composite [80].

4.1.2 Fiber volume fraction and porosity

Although differential swelling behavior was found, as shown in the previous section, the effect of irradiation on the fiber volume fraction was negligible because of the small swelling value (up to ~2% in volume). It is also expected that irradiation will not change the porosity.

4.1.3 Thermal expansion

Since very limited data are available for the CTEs of SiC/SiC composites irradiated under LWR-relevant temperature and dose conditions, this report presents instantaneous CTEs for HNS fiber–reinforced CVI SiC/SiC composite plates neutron-irradiated at 360 or 370°C to 1dpa under an inert atmosphere in the HFIR, as shown in Figure 16. Dilatometry of the irradiated ~24 mm long specimens was conducted using a NETZSCH DIL 402CD horizontal dual pushrod dilatometer with a heating rate of 1°C/min and a cooling rate of 2.5°C/min. It was found that the instantaneous CTE of the neutron-irradiated SiC/SiC was described by the CTE of nonirradiated SiC/SiC composites (Eq. (1)) up to the irradiation temperature, showing that the effect of irradiation on the CTE was insignificant. This is consistent with a previous study of the CTE of SiC/SiC composites irradiated at higher temperatures [5]. Note that, above the irradiation temperature, the CTE was apparently small because of recovery of swelling by defect recovery.

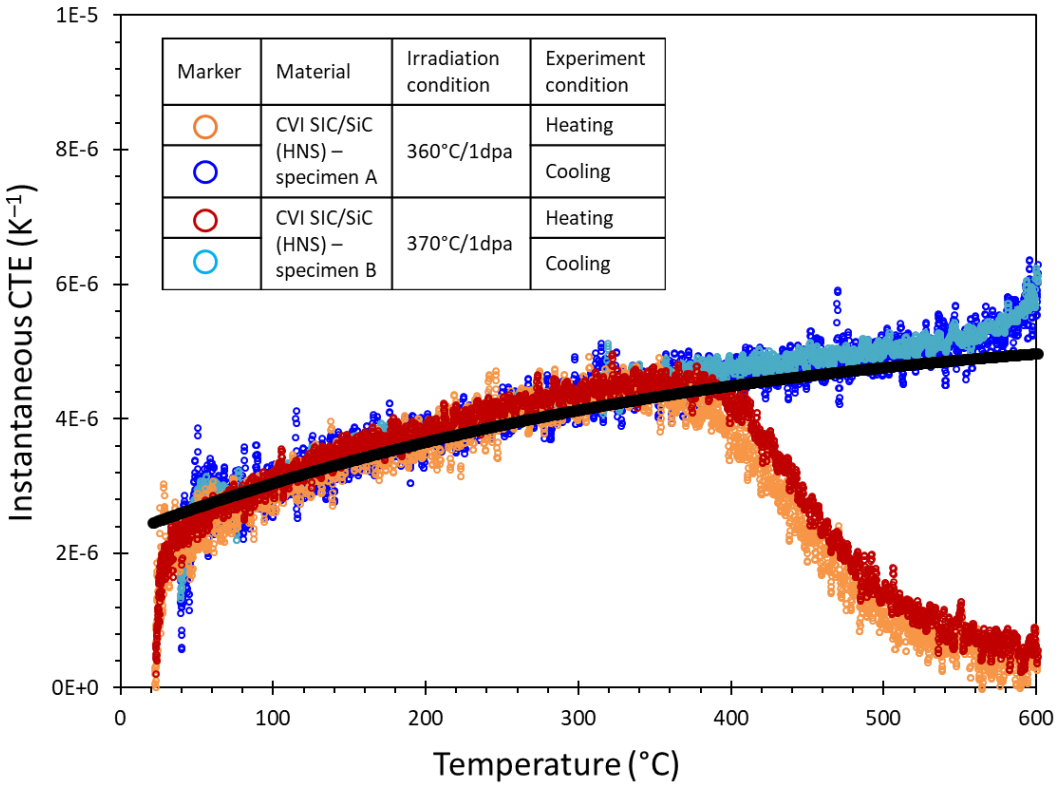

Figure 16. Instantaneous CTE of neutron-irradiated CVI SiC/SiC composite plates. The black line is the trend of nonirradiated materials, which is described in Eq. (1). The material information can be found in [80].

4.1.4 Thermal diffusivity

Since there are no thermal diffusivity data for SiC tubes obtained by a standard method, no reliable thermal properties data are available for neutron-irradiated SiC tubes. In such a situation, it would be reasonable to use the thermal properties obtained from the plate specimens for modeling purposes. The effect of irradiation on the thermal conductivity of ceramics is described by the thermal resistivity, the inverse of thermal conductivity, K [83]:

$$\frac{1}{K_{rd}} = \frac{1}{K_{irr}} - \frac{1}{K_{non-irr}} \quad (6)$$

where $1/K_{irr}$ and $1/K_{non\text{-}irr}$ indicate irradiated and nonirradiated thermal resistivity, respectively, and $1/K_{rd}$ is the radiation defect thermal resistivity that represents collective contributions from various radiation-produced defects to the volume thermal resistivity.

Figure 17a shows the room-temperature defect thermal resistivity of SiC/SiC plate specimens and monolithic CVD SiC [5], together with the defect thermal resistivity of neutron-irradiated SiC tubes evaluated by the laser flash method with a curved specimen [7]. The appearance of the tube specimen used for the diffusivity test is shown in Figure 17b. This study also provides preliminary result of the defect thermal resistivity determined based on thermal diffusivity of a curved specimen made of CVI SiC/SiC composite neutron irradiated to 2.3 dpa under a radial heat flux of ~0.7 MW/m^2 [82]. It is clear that the defect thermal resistivity of the plate specimens is material-dependent. The results from the tube specimens reported in [7] appeared to be consistent with the results from the plate specimens. Note that the triplex tube specimen [7] was expected to be greatly affected by the monolithic layer because of its volume fraction. The dose dependence of irradiation thermal defect resistivity can be obtained from a linear relationship between the thermal defect resistivity and the swelling [54].

Because very limited thermal properties data for the SiC/SiC cladding are available, future work on this topic requires (1) the development of a standard test method for the thermal properties evaluation of ceramic tubes, (2) an evaluation of the thermal properties of SiC-based tubes irradiated under LWR-relevant temperatures and doses, and (3) modeling or theoretical description of thermal diffusivity of SiC tube based on its microstructure to predict the thermal property of different SiC composite tubes.

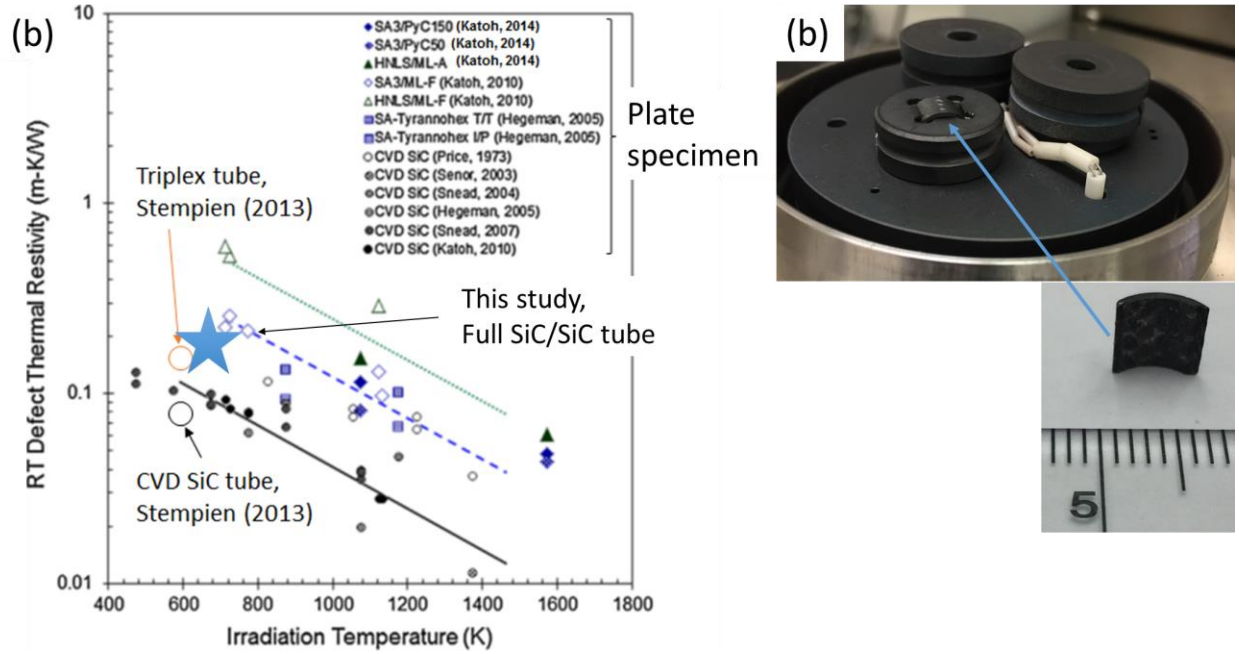

Figure 17. (a) Room-temperature radiation defect thermal resistivity of neutron-irradiated SiC/SiC composites and monolithic CVD SiC plotted against irradiation temperature [5, 7]. The neutron dose ranged from 0.8 to 11.7 dpa for composites. This study evaluated the defect resistivity of CVI full SiC/SiC composite tube with HNS fibers neutron irradiated 2.3 dpa. (b) appearance of test apparatus and machined SiC/SiC tube specimen for thermal diffusivity test.

4.1.5 Specific heat

The effect of neutron irradiation on the specific heat of the SiC/SiC tube was negligible because of the limited change in the density following irradiation.

4.1.6 Stored energy

The production of Frenkel pairs in graphite by neutron irradiation was postulated by E.P. Wigner in 1942. Later, it was pointed out by Szilard that when these defects recombined the defect formation energy of approximately 8 eV will be released. These two phenomena became known as the Wigner Effect and the Szilard Complication, respectively. The energy released during recovery of Frenkel pairs is so called the Wigner energy. The potential danger of stored energy release during reactor operation was discovered early in the operation of the air-cooled graphite reactors at Windscale in the United Kingdom. To prevent the build-up of excessive amounts of stored energy the reactors were routinely thermal annealed to reduce the extent of the 200°C release peak. However, the 1957 Windscale Reactor 1 fire was initialed by the anomalous stored energy release during one of these scheduled anneals.

Although stored energy release is not unique to graphite, in practical terms, no other nuclear ceramics has an issue with the Wigner energy. Given the relatively high energy for defect recombination and relevance to nuclear energy, the Wigner energy potential for SiC was investigated by Primak in 1956 [84]. Though this work concluded that the stored energy release of SiC was not significant, the neutron dose was only ~0.04 dpa. Therefore, it is necessary to conduct systematic evaluation of stored energy in SiC irradiated with different temperature and neutron dose. Stored energy is especially important for SiC

cladding in case of an accident where a high ramping rate of temperature has the stored energy release in a short period of time.

4.1.7 Permeability

At this point, there is no report on the permeability of SiC/SiC composites in tubular configurations subject to neutron irradiation. This study reports the gas permeability of neutron-irradiated CVD SiC tubes following neutron irradiation at ~300°C to ~2 dpa with a high heat flux. Detailed material information and irradiation conditions can be found elsewhere [82]. Following the same procedure used in testing of nonirradiated samples shown in Hu et al. (2017) [57], the helium and deuterium permeation flux through a neutron-irradiated CVD SiC tube was measured. The results, shown in Figure 18, indicate that the tested CVD SiC tubular sample following neutron irradiation is still hermetic, as manifested by the extremely low helium and deuterium permeation fluxes at various gas pressures. This finding implies that CVD SiC–coated SiC/SiC cladding is hermetic following neutron irradiation.

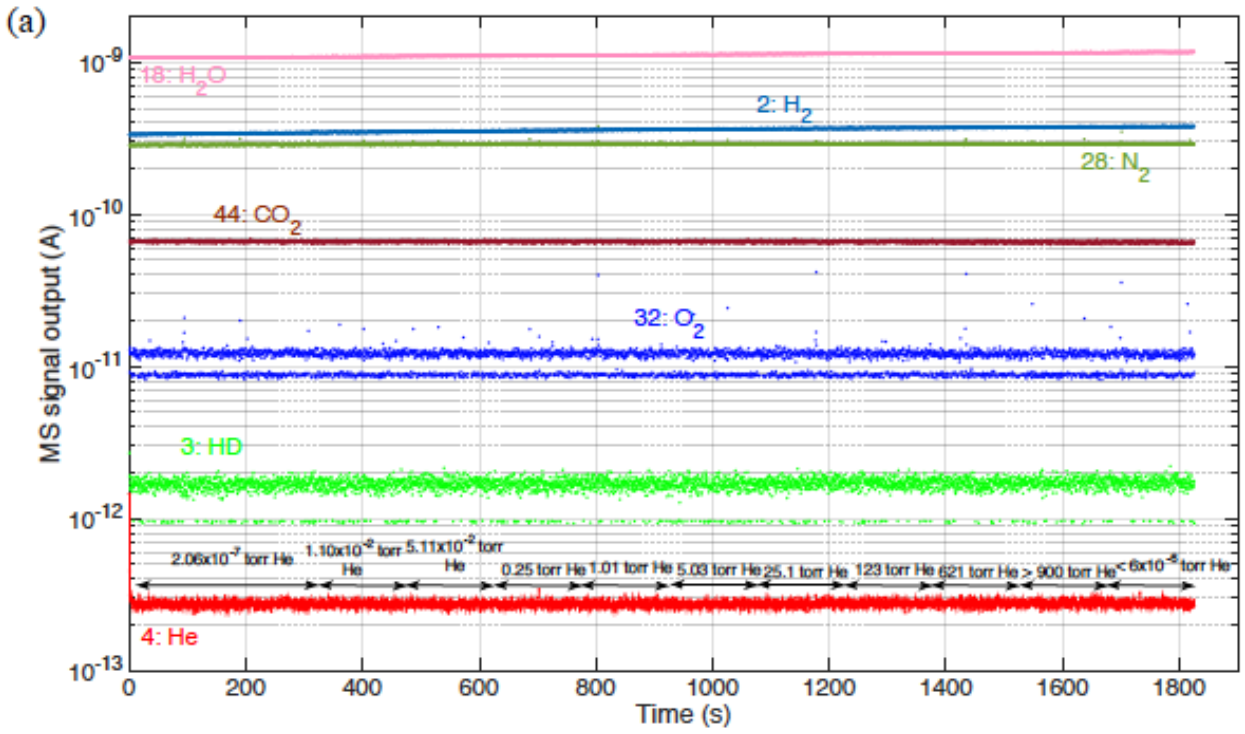

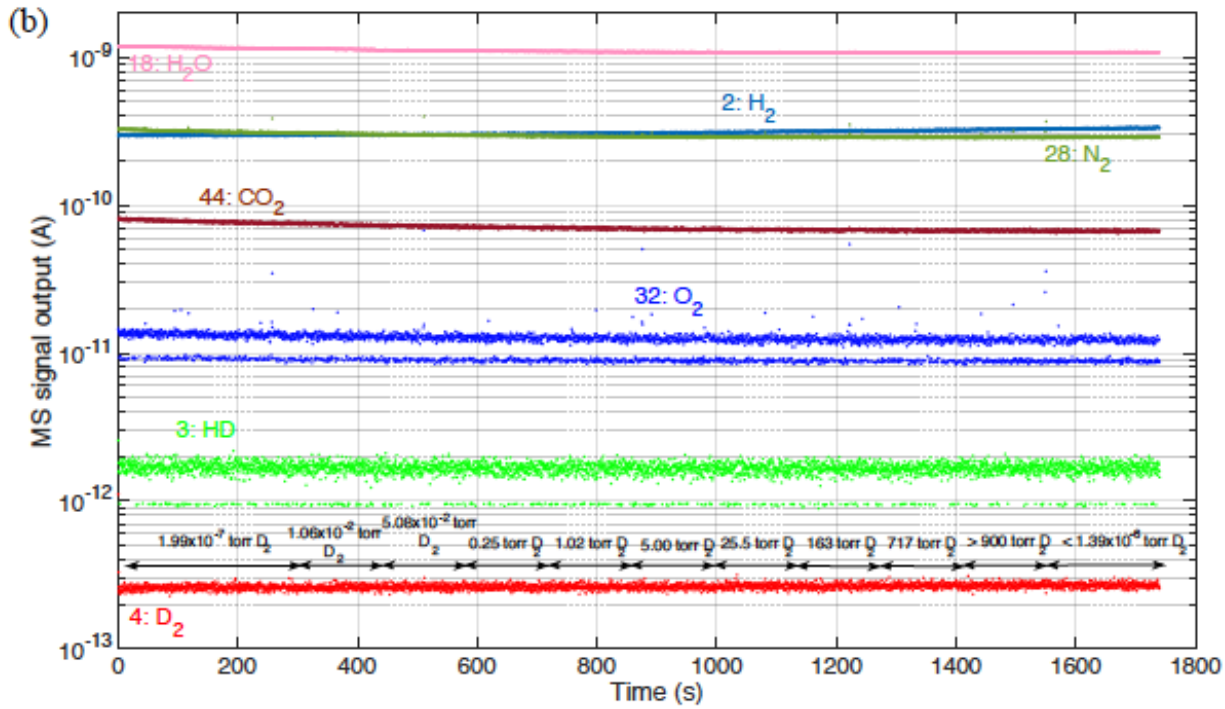

Figure 18. (a) Helium and (b) deuterium permeation fluxes through neutron-irradiated CVD SiC as a function of applied gas pressure [57].

4.2 Mechanical Properties

Since mechanical properties date for irradiated SiC/SiC tubes are highly limited, the mechanical properties of irradiated SiC/SiC composite plates are presented. Table 10 lists the reported mechanical properties of SiC/SiC plates neutron-irradiated under LWR-relevant dose and temperature conditions. Although the available data are limited, Table 10 shows that no notable irradiation-induced degradation of mechanical properties (e.g., Young's modulus, PLS, ultimate strength) was found for CVI SiC/SiC composites with SA3 or HNS coated multi-layer or single-layer PyC. Recent work [81] shows no notable effect of irradiation at ~300°C up to 11.8 dpa on the flexural behavior of CVI SiC/SiC composites with monolayer PyC-coated HNS or SA3 fibers (Figure 18). Although the effect of irradiations on elastic modulus were insignificant, it was observed that the average Young's modulus tended to decreased by up to ~10% following neutron irradiation at below ~1000°C (Figure 20) [5]. For prediction of this change, previous study recommended that a linear relationship between the Young's modulus decrease and the linear swelling with a correlation factor of ~10, which means ~7% decrease in Young's modulus at 300°C after the swelling saturation at slightly over 2% in volume [5]. As explained above, it is reasonable to assume that the effects of irradiation on the mechanical properties are negligible for modeling during normal operation, except for slight reduction of Young's modulus. However, mechanical degradation may be taken into account in the model at high doses because both HNS fiber and multi-layer PyC/SiC interphase were degraded at a high dose of ~40 dpa at 300 and 500°C [85]. Currently, no data are available for the mechanical properties of NITE SiC/SiC composites, although the tensile properties were retained following neutron irradiation at 600°C to 0.52 dpa, at 830°C to 5.9 dpa, and at 1270°C to 5.8 dpa [86]. The statistical strengths were also investigated for flat coupons of CVI SiC/SiC composites following neutron irradiation. In short, the effects of neutron irradiation on the statistical strength properties do not appear significant for both PLS and UTS though the data is highly limited [5].

Irradiation creep is known to be a key property for modeling the stress state under irradiation. In short, and especially for SiC materials that possess very limited strain tolerance, irradiation creep provides an important stress mitigating function. Neutron irradiation creep of SiC materials was investigated up to 30 dpa using a bend stress relaxation technique [87]. This study found that irradiation creep of various SiC materials (different grades of CVD SiC ceramics, nano-powder sintered SiC ceramics, SiC fibers, and NITE SiC/SiC composites) was described by swelling-coupled transient creep and post-transient creep with a creep coefficient of ~1×10^{-7} [MPa^{-1} dpa^{-1}] with a few exceptions for single-crystal materials and SiC materials with a strong grain texture. This study also found similar relaxation creep behavior among NITE SiC/SiC composites, SiC fibers (HNS and SA3), and CVD SiC. This paper recommends use of the creep coefficient of CVD SiC for modeling of CVI SiC/SiC composite cladding because of a lack of data. Current knowledge is that irradiation creep strain of SiC is significantly limited compared with the swelling. Therefore, the swelling dominantly determines the dimensional stability under irradiation, and irradiation creep strain can be ignored for modeling according to current database. It is necessary to obtain irradiation creep data of CVI SiC/SiC composites under stresses both below and beyond PLS.

Table 9. Mechanical properties of CVI SiC/SiC composites nonirradiated and irradiated under LWR-relevant temperature and dose conditions. All the irradiation experiments were carried out under an inert gas atmosphere in the HFIR

Material (Interphase type)	Irradiation conditions	Test method	Young's modulus (GPa)	Proportional limit stress (MPa)	Ultimate strength (MPa)	Reference
HNS CVI SiC/SiC plate ($PyC_{20\ nm}/SiC_{100\ nm}$ multi-layer)	Nonirradiated 1 Nonirradiated 2 570°C/2.2 dpa	Cyclic tensile	232 (25) 226 (27) 197 (19)	97 (24) 126 (12) 116 (12)	284 (19) 224(13) 171 (38)	[88]
HNS CVI SiC/SiC plate ($PyC_{20\ nm}/SiC_{100\ nm}$ multi-layer)	Nonirradiated 300°C/3.4 dpa	4 point flexural	Not available	375.0 (50.9) 332.4 (4.5)	469.9 (70.1) 420.4 (29.8)	[89]
HNS CVI SiC/SiC plate (PyC 50–160 nm)	Nonirradiated	Dynamic modulus 4 point flexural	255 (6)	216 (8)	412 (35)	[81]
	280–340°C/2.0 dpa		236 (24)	260 (28)	509 (49)	
	230–280°C/11.8 dpa		210 (13)	226 (45)	486 (72)	
SA3 CVI SiC/SiC plate (PyC 200–350 nm)	Nonirradiated	Dynamic modulus 4 point flexural	241 (11)	331 (91)	493 (59)	[81]
	280–340°C/2.0 dpa		241 (22)	300 (40)	513 (87)	
	230–280°C/11.8 dpa		220 (7)	344 (85)	482 (74)	

Note: values in brackets are standard deviations.

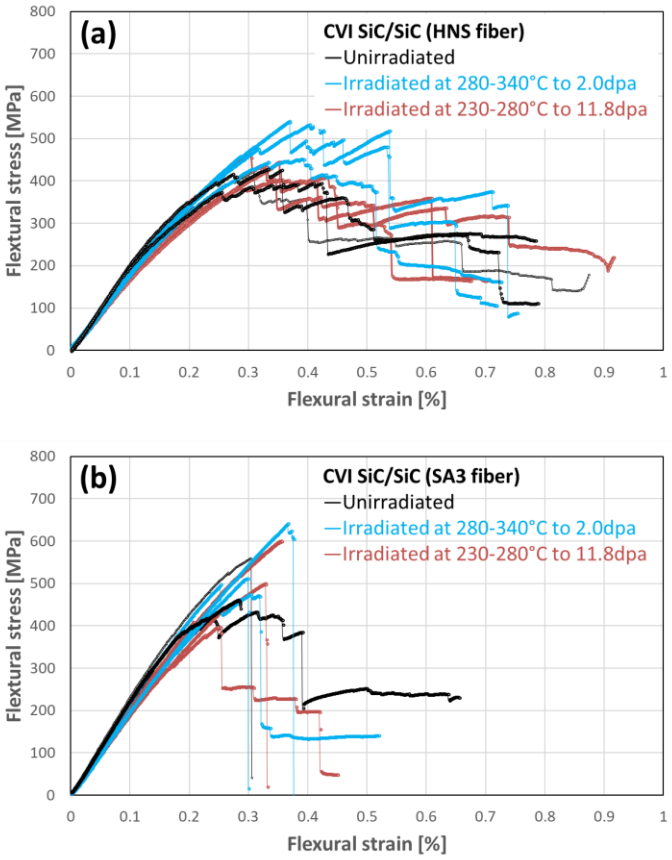

Figure 19. Flexural stress strain curves for (a) CVI SiC/SiC (HNS)-C and (b) CVI SiC/SiC (SA3) for nonirradiated and irradiated conditions [81].

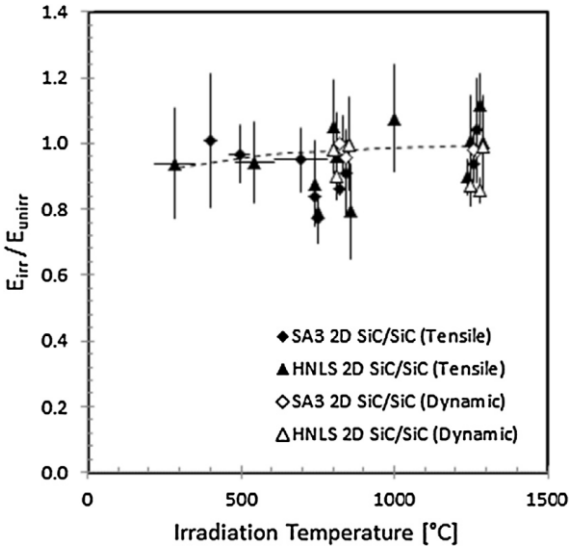

Figure 20. Tensile and dynamic Young's moduli for irradiated CVI SiC/SiC composites normalized to the unirradiated values. Note that flat coupon specimens were used for testing. The figure was reprinted from [5].

Effects of irradiation on the strength of selected SiC plate to plate joints are summarized in Table 11 [24, 90]. The irradiation was conducted at 280–310°C to 8.7 dpa, which is relevant to LWR applications. The substrate was monolithic CVD SiC for all the cases. Torsional shear testing using a miniature hourglass specimen was conducted. It is noted that the obtained strength is apparent because of nonuniform stress distribution within the specimen during the testing. Details of the interpretation of the torsion strength can be found elsewhere [91, 92]. As shown in Table 11, all of the joints exhibited relatively high values (>80 MPa on average) of apparent shear strength following neutron irradiation. However, irradiation-induced cracking within the bonding layer typically was found in the non-SiC bonding layers. Although the strength of the cracked joint was relatively high, the cracking may result in the loss of the gas leak tightness of the joints. Future work is needed to demonstrate robust and hermetic SiC joints with an end-plug configuration, since the bonding quality may be different between plate-to-plate joints and end-plug joints.

Table 10. Apparent shear strength of various SiC joints with and without irradiation. The substrate was monolithic CVD SiC for all cases. Torsion tests using a miniature hourglass specimen were conducted to obtain the data.

Joining method (joint phases)	Conditions	Apparent shear strength [MPa]	Note	Reference
Titanium foil diffusion (Ti_3SiC_2, $TiSi_2$)	Nonirradiated Irradiated at 280–310°C to 8.7 dpa	133 (22) 86 (66)	Irradiation-induced cracking	[90]
Molybdenum foil diffusion ($Mo_{<5}Si_3C_{<1}$, Mo_2C)	Nonirradiated Irradiated at 280–310°C to 8.7 dpa	146 (14) 84 (6)		
SiC nanopowder slurry sintering (SiC, Y-Al-Zr oxides)	Nonirradiated Irradiated at 280–310°C to 8.7 dpa	320 (31) 226 (156)	No obvious microstructural change by irradiation	
SiC nano-powder green sheet sintering (SiC, Y-Al-Zr oxides)	Nonirradiated Irradiated at 280–310°C to 8.7 dpa	116 (24) 109 (54)		
Ti-Si-C reaction sintering (Ti_3SiC_2, SiC, minor TiC)	Nonirradiated Irradiated at 280–310°C to 8.7 dpa	147 (12) 123 (13)	Irradiation-induced cracking	
Hybrid polymer/CVI SiC (SiC)	Nonirradiated Irradiated at 280–310°C to 8.7 dpa	93 (12) 93 (17)	No obvious microstructural change by irradiation	
Brazing (Al-Si-C-O)	Nonirradiated Irradiated at 280–310°C to 8.7 dpa	138 (20) 190 (10)	No obvious microstructural change by irradiation*	[24]

*Unpublished result

Note: values in brackets are standard deviation

4.3 In-Pile Hydrothermal Corrosion

Neutron irradiation is an important factor affecting hydrothermal corrosion; the radiolysis of light water increases the concentrations of oxidizing radiolytic species [93], and irradiation-induced defects may

change the reactivity of the material. Previous in-pile tests at the Massachusetts Institute of Technology reactor—with open-ended CVI SiC/SiC composite tube samples in a simulated PWR coolant with 10.3 MPa pressure at 300°C—showed a significant increase in weight loss compared with corrosion without irradiation [7]. An autoclave test with ion-irradiated CVD SiC samples also indicated accelerated corrosion with irradiation. Although the data are limited, irradiation-assisted corrosion of the SiC likely occurred. Stempien et al. (2013) reported in-pile corrosion behaviors in SiC plate joints bonded with TiC/SiC tape, calcium aluminate glass, or titanium foil [7]. All types of these joints were completely or partially debonded during the simulated PWR reactor coolant exposure for 44 days at an irradiation dose of up to 0.16 dpa for SiC. Although the presence of irradiation-enhanced corrosion is not clearly addressed in Stempien et al. [7], the development of a corrosion-tolerant joint is a critical issue. The in-pile corrosion behavior of coatings also is rarely reported.

The current state of knowledge in the area of corrosion of SiC fuel cladding in LWR coolant environments is very shallow, presenting what is perhaps the biggest current knowledge gap for this technology. Systematic tests with well-defined samples, under well-known conditions, aiming to quantify the kinetics and identify the mechanism for corrosion, are necessary.

5. FUTURE DIRECTIONS

This report summarized various physical, mechanical, and chemical compatibility properties of SiC/SiC composites for LWR cladding applications. To provide relatively complete information for SiC/SiC composites (the ultimate purpose of this handbook), other properties need to be added in future publications. The important data gaps identified in the process of compiling the present report include the followings.

Thermo-physical properties: While physics of thermal conductivity and the neutron irradiation effects on it are well understood, detailed understanding of the constitutive properties is still lacking. In order to achieve a high fidelity modeling capability for thermal conductivity of SiC/SiC composite fuel claddings as a function of temperature and neutron dose, data and analysis for the SiC/SiC cladding tube thermal conductivity coupled with detailed tomography information for individual test specimens are needed.

Gas tightness: Presently the gas permeability data for prototypical SiC/SiC composite fuel cladding tubes are extremely limited. Additional data in pristine and irradiated (under relevant heat flux) conditions will be essential to better address the magnitude of gas tightness issue for SiC/SiC composite claddings. Since the gas permeation through SiC/SiC composite wall is a statistical phenomenon governed by development of microcrack networks, studies on this issue need to be coupled with the mechanical properties and the thermo-mechanical analysis.

Elastic constants: It is desirable to acquire the full stiffness matrix data for the prototypical tube materials. In addition, establishing methods for the experimental determination of the full stiffness matrix and the modeling capability based on the micro- and meso-scopic material information will be useful. Credible data for neutron-irradiated prototypical tubes are still missing.

Mechanical properties: There are significant gaps for mechanical properties data and analytical/predictive capabilities. The main data needs are related to the multi-axial failure, loss of gas tightness, statistical failure properties, and pellet-clad mechanical interactions. Specific needs include 1) extensive database and analysis to establish the multi-axial failure criteria for prototypical SiC/SiC tubes, 2) data, modeling capability, and theoretical basis for predicting probability of through-wall microcrack network development, and 3) mechanical properties data and understanding relevant to PCMI including the reactivity-initiated accident.

Irradiation creep: Data on creep behavior under neutron irradiation are entirely missing for the prototypical SiC/SiC composite materials. In addition, the existing irradiation creep data for the matrix materials and reinforcing SiC fibers are not sufficient in terms of both quantity and consistency.

Stored energy release and related phenomena: Presently data for stored energy and its release from neutron-irradiated SiC are limited to those from experiments at irrelevant irradiation temperature. Hence, data from experiments at relevant conditions are needed. Moreover, experimental data for various phenomena related with the thermal annealing of irradiation defects are largely missing. Such data include the recovery rates for swelling, thermal conductivity, and elastic modulus in addition to the associated energy release rate.

In-pile hydrothermal corrosion: The practical reactor core environment may strongly influence the hydrothermal corrosion behavior of materials due to the simultaneous presence of water radiolysis and radiation damage. Due to the complex nature of the phenomena, data from highly controlled experiments under rigorous quality assurance and diverse material quality (intrinsic defects, impurities, etc.) will be most useful. Fundamental knowledge about the governing mechanisms is insufficient, too.

Fuel compatibility: While the UO_2 – SiC chemical compatibility is reasonably understood and considered a non-threat at normal operating temperatures, the system is known to be reactive at very high temperatures. A comprehensive survey of the UO_2 – SiC PCCI will be useful to identify any important studies in near future. Data on chemical compatibility of SiC with other fuel forms are needed, shall such fuels be considered.

Steam oxidation: Steam oxidation behavior of SiC/SiC composites in simulated beyond-design basis accident scenarios has been addressed positively. The steam pressure dependence of SiC oxidation remains to be sufficiently understood. Moreover, although it is outside scope of the present document, data for steam oxidation behaviors of SiC/SiC composites with coatings of dissimilar materials are largely missing.

ACKNOWLEDGMENTS

The authors would like to thank Jeffery Powers and Yoonjo Lee at ORNL for critical review of the report. The research is sponsored by the Advanced Fuels Campaign of the Nuclear Technology R&D program, Office of Nuclear Energy, DOE, under contract DE-AC05-00OR22725 with UT-Battelle, LLC. A portion of this research used resources at the HFIR, a DOE Office of Science User Facility operated by ORNL. This work also used resources at the Low Activation Materials Development and Analysis Laboratory at ORNL.

6. REFERENCES

[1] S.J. Zinkle, K.A. Terrani, J.C. Gehin, L.J. Ott, L.L. Snead, Accident tolerant fuels for LWRs: A perspective, J. Nucl. Mater. 448 (2014) 374–379.

[2] K.A. Terrani, B.A. Pint, C.M. Parish, C.M. Silva, L.L. Snead, Y. Katoh, Silicon carbide oxidation in steam up to 2 MPa, J. Am. Ceram. Soc. 97 (2014) 2331–2352.

[3] Y. Katoh, L.L. Snead, I. Szlufarska, W.J. Weber, Radiation effects in SiC for nuclear structural applications, Curr. Opin. Solid State Mater. Sci. 16 (2012) 143–152.

[4] K.A. Terrani, Accident tolerant fuel cladding development: Promise, status, and challenges, J. Nucl. Mater. 501 (2018) 13–30.

[5] Y. Katoh, K. Ozawa, C. Shih, T. Nozawa, R.J. Shinavski, A. Hasegawa, L.L. Snead, Continuous SiC fiber, CVI SiC matrix composites for nuclear applications: Properties and irradiation effects, J. Nucl. Mater. 448 (2014) 448–476.

[6] C.P. Deck, G.M. Jacobsen, J. Sheeder, O. Gutierrez, J. Zhang, J. Stone, H.E. Khalifa, C.A. Back, Characterization of SiC-SiC composites for accident tolerant fuel cladding, J. Nucl. Mater. 466 (2015) 1–15.

[7] J.D. Stempien, D.M. Carpenter, G. Kohse, M.S. Kazimi, Characteristics of Composite Silicon Carbide Fuel Cladding after Irradiation under Simulated PWR Conditions, Nucl. Technol. 183 (2013) 13–29.

[8] D. Kim, H.G. Lee, J.Y. Park, W.J. Kim, Fabrication and measurement of hoop strength of SiC triplex tube for nuclear fuel cladding applications, J. Nucl. Mater. 458 (2015) 29–36.

[9] Y.-H. Koo, KAERI's Development of LWR Accident-Tolerant Fuel, Nucl. Technol. (2014). doi:10.13182/NT13-89.

[10] C. Ang, C. Kemery, Y. Katoh, Electroplating chromium on CVD SiC and SiCf-SiC advanced cladding via PyC compatibility coating, J. Nucl. Mater. 503 (2018) 245–249.

[11] C. Sauder, Ceramic Matrix Composites: Nuclear Applications, in: Ceram. Matrix Compos. Mater. Model. Technol., 2014: pp. 609–646.

[12] L.L. Snead, D. Steiner, S.J. Zinkle, Measurement of the effect of radiation damage to ceramic composite interfacial strength, J. Nucl. Mater. 191–194 (1992) 566–570.

[13] J.A. DiCarlo, H.-M. Yun, Non-oxide (Silicon Carbide) Fibers, in: Handb. Ceram. Compos., Springer US, 2005: pp. 33–52.

[14] Y. Katoh, T. Nozawa, L.L. Snead, Mechanical properties of thin pyrolitic carbon interphase SiC-matrix composites reinforced with near-stoichiometric SiC fibers, J. Am. Ceram. Soc. 88 (2005) 3088–3095.

[15] J. Lamon, Chemical Vapor Infiltrated SiC/SiC Composites (CVI SiC/SiC), in: Handb. Ceram. Compos., Springer US, n.d.: pp. 55–76.

[16] T. Hinoki, Y. Katoh, L.L. Snead, H.-C. Jung, K. Ozawa, H. Katsui, Z.-H. Zhong, S. Kondo, Y.-H. Park, C. Shih, C.M. Parish, R.A. Meisner, A. Hasegawa, Silicon Carbide and Silicon Carbide Composites for Fusion Reactor Application, Mater. Trans. 54 (2013) 472–476.

[17] C.P. Deck, H.E. Khalifa, B. Sammuli, T. Hilsabeck, C.A. Back, Fabrication of SiC-SiC composites for fuel cladding in advanced reactor designs, in: Prog. Nucl. Energy, 2012: pp. 38–45.

[18] Y. Katoh, S.M. Dong, A. Kohyama, Thermo-mechanical properties and microstructure of silicon carbide composites fabricated by nano-infiltrated transient eutectoid process, in: Fusion Eng. Des., 2002: pp. 723–731.

[19] A. Kohyama, "Inspire" Project for R&D of Sic/Sic Fuel Cladding by Nite Method, in: Ceram. Environ. Energy Appl. II, John Wiley & Sons, Inc., Hoboken, NJ, USA, 2014: pp. 99–107.

[20] C.M. Parish, K.A. Terrani, Y.-J. Kim, T. Koyanagi, Y. Katoh, Microstructure and hydrothermal corrosion behavior of NITE-SiC with various sintering additives in LWR coolant environments, J. Eur. Ceram. Soc. 37 (2017) 1261-1279.

[21] Z. Duan, H. Yang, Y. Satoh, K. Murakami, S. Kano, Z. Zhao, J. Shen, H. Abe, Current status of materials development of nuclear fuel cladding tubes for light water reactors, Nucl. Eng. Des. 316 (2017) 131–150.

[22] I. Spitsberg, J. Steibel, Thermal and Environmental Barrier Coatings for SiC/SiC CMCs in Aircraft Engine Applications, Int. J. Appl. Ceram. Technol. 1 (2005) 291–301.

[23] C.K. Ang, K. Terrani, J. Burns, Y. Katoh, Examination of Hybrid Metal Coatings for Mitigation of Fission Product Release and Corrosion Protection of LWR SiC/SiC, Oak Ridge, 2016. ORNL/TM-2016/332

[24] J.R. Fellows, C.A. Lewinsohn, Y. Katoh, T. Koyanagi, Low temperature air braze process for joining silicon carbide components used in heat exchangers, fusion and fission reactors, and other energy production and chemical synthesis systems, in: Ceram. Eng. Sci. Proc., 37 [6] (2017) 3–16.

[25] H.E. Khalifa, C.P. Deck, O. Gutierrez, G.M. Jacobsen, C.A. Back, Fabrication and characterization of joined silicon carbide cylindrical components for nuclear applications, J. Nucl. Mater. 457 (2015) 227–240.

[26] J.J. Sha, T. Nozawa, J.S. Park, Y. Katoh, A. Kohyama, Effect of heat treatment on the tensile strength and creep resistance of advanced SiC fibers, J. Nucl. Mater., 329 (2004) 592–596.

[27] T.J. Moore, Feasibility Study of the Welding of Sic, J. Am. Ceram. Soc. 68 (1985) C‐151-C‐151.

[28] D. DeLeeuw, Effects of Joining Pressure and Deformation on the Strength and Microstructure of Diffusion-Bonded Silicon Carbide, J. Am. Ceram. Soc. 75 (1992) 725–727.

[29] B. V Cockeram, The Diffusion Bonding of Silicon Carbide and Boron Carbide Using Refractory Metals. https://www.osti.gov/servlets/purl/755392

[30] Y. Jung, J.H. Park, H.G. Kim, D.J. Park, J.Y. Park, W.J. Kim, Effect of Ti and Si Interlayer Materials on the Joining of SiC Ceramics, Nucl. Eng. Technol. 48 (2016) 1009–1014.

[31] J.R. McDermid, R.A.L. Drew, Thermodynamic Brazing Alloy Design for Joining Silicon Carbide, J. Am. Ceram. Soc. 74 (1991) 1855–1860.

[32] Y. Liu, Z.R. Huang, X.J. Liu, Joining of sintered silicon carbide using ternary Ag-Cu-Ti active brazing alloy, Ceram. Int. 35 (2009) 3479–3484.

[33] W. Lippmann, J. Knorr, R. Wolf, R. Rasper, H. Exner, A.M. Reinecke, M. Nieher, R. Schreiber, Laser joining of silicon carbide - A new technology for ultra-high temperature resistant joints, Nucl. Eng. Des. 231 (2004) 151–161.

[34] M. Ferraris, M. Salvo, V. Casalegno, S. Han, Y. Katoh, H.C. Jung, T. Hinoki, A. Kohyama, Joining of SiC-based materials for nuclear energy applications, J. Nucl. Mater., 417 [1-3] (2011) 379–382.

[35] P. Colombo, V. Sglavo, E. Pippel, J. Woltersdorf, Joining of reaction-bonded silicon carbide using a preceramic polymer, J. Mater. Sci. 33 (1998) 2405–2412.

[36] C.A. Lewinsohn, R.H. Jones, P. Colombo, B. Riccardi, Silicon carbide-based materials for joining silicon carbide composites for fusion energy applications, J. Nucl. Mater. 307–311 (2002) 1232–1236.

[37] M. Singh, Microstructure and mechanical properties of reaction-formed joints in reaction-bonded silicon carbide ceramics, J. Mater. Sci. 33 (1998) 5781–5787.

[38] C.H. Henager, R.J. Kurtz, Low-activation joining of SiC/SiC composites for fusion applications, J. Nucl. Mater. 417 [1-3] (2011) 375–378.

[39] T. Koyanagi, Y. Katoh, K.A. Terrani, Y.-J. Kim, J.O. Kiggans, T. Hinoki, Hydrothermal corrosion of silicon carbide joints without radiation, J. Nucl. Mater. 481 (2016) 226–233.

[40] T. Hinoki, N. Eiza, S. Son, K. Shimoda, J. Lee, A. Kohyama, Development of Joining and Coating Technique for SiC and SiC/SiC Composites Utilizing NITE Processing, Mech. Prop. Perform. Eng. Ceram. Compos. Ceram. Eng. Sci. Proceedings, 26 (2005) 399–405.

[41] T. Iseki, K. Arakawa, H. Suzuki, Joining of dense silicon carbide by hot-pressing, J. Mater. Sci. 15 (1980) 1049–1050.

[42] W.D. Kingery, Densification during sintering in the presence of a liquid phase. I. Theory, J. Appl. Phys. 30 (1959) 301–306.

[43] K. Shimoda, N. Eiza, J.-S. Park, T. Hinoki, A. Kohyama, S. Kondo, High-Temperature Mechanical Property Improvements of SiC Ceramics by NITE Process, Mater. Trans. 47 (2006) 1204–1208.

[44] G. Singh, S. Gonczy, C. Deck, E. Lara-Curzio, Y. Katoh, Interlaboratory round robin study on axial tensile properties of SiC-SiC CMC tubular test specimens, Int. J. Appl. Ceram. Technol. (2018). doi:10.1111/ijac.13010.

[45] F. Bernachy-Barbe, L. Gélébart, M. Bornert, J. Crépin, C. Sauder, Anisotropic damage behavior of SiC/SiC composite tubes: Multiaxial testing and damage characterization, Compos. Part A Appl. Sci. Manuf. 76 (2015) 281–288.

[46] J. Zhang, H.E. Khalifa, C. Deck, J. Sheeder, C.A. Back, Thermal Diffusivity Measurement of Curved Samples Using the Flash Method, Ceram. Eng. Sci. Proceedings, 36 [7] (2015) 43–56.

[47] K. Shapovalov, G.M. Jacobsen, L. Alva, N. Truesdale, C.P. Deck, X. Huang, Strength of SiCf-SiCm composite tube under uniaxial and multiaxial loading, J. Nucl. Mater. 500 (2018) 280–294.

[48] E. Rohmer, E. Martin, C. Lorrette, Mechanical properties of SiC/SiC braided tubes for fuel cladding, J. Nucl. Mater. 453 (2014) 16–21.

[49] D. Hayasaka, J.S. Park, H. Kishimoto, A. Kohyama, Gas leak tightness of SiC/SiC composites at elevated temperature, Fusion Eng. Des. 109–111 (2016) 1498–1501.

[50] L. Alva, K. Shapovalov, G.M. Jacobsen, C.A. Back, X. Huang, Experimental study of thermo-mechanical behavior of SiC composite tubing under high temperature gradient using solid surrogate, J. Nucl. Mater. 466 (2015) 698–711.

[51] D. Hayasaka, J.S. Park, H. Kishimoto, A. Kohyama, Gas leak tightness of SiC/SiC composites at elevated temperature, Fusion Eng. Des. 109–111 (2016) 1498–1501.

[52] D. Hayasaka, H. Kishimoto, A. Kohyama, Helium permeability of high-performance SiC/SiC tube, J. Nucl. Sci. Technol. 53 [12] (2016) 2034–2039.

[53] K.A. Terrani, J.O. Kiggans, C.M. Silva, C. Shih, Y. Katoh, L.L. Snead, Progress on matrix SiC processing and properties for fully ceramic microencapsulated fuel form, J. Nucl. Mater. 457 (2015) 9–17.

[54] L.L. Snead, T. Nozawa, Y. Katoh, T.S. Byun, S. Kondo, D.A. Petti, Handbook of SiC properties for fuel performance modeling, J. Nucl. Mater. 371 (2007) 329–377.

[55] Y. Yamamoto, Y. Murakami, H. Yamaguchi, T. Yamamoto, D. Yonetsu, K. Noborio, S. Konishi, Re-evaluation of SiC permeation coefficients at high temperatures, Fusion Eng. Des. 109–111 (2016) 1286–1290.

[56] Y. Katoh, L.L. Snead, C.M. Parish, T. Hinoki, Observation and possible mechanism of irradiation induced creep in ceramics, J. Nucl. Mater. 434 (2013) 141–151.

[57] Xunxiang Hu, Takaaki Koyanagi, Gyanender P. Singh, Yutai Katoh, Determination of He and D permeability of neutron irradiated SiC tubes to examine the potential for release due to microcracking, 2017. https://info.ornl.gov/sites/publications/Files/Pub293363.pdf.

[58] T. Nozawa, K. Ozawa, Y.B. Choi, A. Kohyama, H. Tanigawa, Determination and prediction of axial/off-axial mechanical properties of SiC/SiC composites, Fusion Eng. Des., (2012) 803–807.

[59] G. Singh, T. Koyanagi, C. Petrie, K. Terrani, Y. Katoh, Evaluating the irradiation effects on the elastic properties of miniature monolithic SiC tubular specimens, J. Nucl. Mater. 499 (2018) 107–110.

[60] ASTM International. ASTM C1773: Standard Test Method for Monotonic Axial Tensile Behavior of Continuous Fiber-Rein-forced Advanced Ceramic Tubular Test Specimens at Ambient Temperature. Annual Book of ASTM Standards. West Conshohocken, PA: ASTM International; 2013.

[61] M. Ben-Belgacem, V. Richet, K.A. Terrani, Y. Katoh, L.L. Snead, Thermo-mechanical analysis of LWR SiC/SiC composite cladding, J. Nucl. Mater. 447 (2014) 125–142.

[62] T. Nozawa, K. Ozawa, C.H. Park, J.-S. Park, A. Kohyama, A. Hasegawa, S. Nogami, T. Hinoki, S. Kondo, T. Yano, T. Shibayama, B. Tsuchiya, T. Shikama, S. Nagata, T. Tanaka, H. Iwakiri, Y. Yamamoto, S. Konishi, R. Kasada, M. Kondo, T. Kunugi, T. Yokomine, Y. Ueki, N. Okubo, T. Taguchi, H. Tanigawa, Japanese activities of the R&D on silicon carbide composites in the broader approach period and beyond, J. Nucl. Mater. (2018) https://doi.org/10.1016/j.jnucmat.2018.05.045

[63] K.A. Terrani, Y. Yang, Y.J. Kim, R. Rebak, H.M. Meyer, T.J. Gerczak, Hydrothermal corrosion of SiC in LWR coolant environments in the absence of irradiation, J. Nucl. Mater. 465 (2015) 488–498.

[64] D. Kim, H.G. Lee, J.Y. Park, J.Y. Park, W.J. Kim, Effect of dissolved hydrogen on the corrosion behavior of chemically vapor deposited SiC in a simulated pressurized water reactor environment, Corros. Sci. 98 (2015) 304–309.

[65] H.-G. Kim, ll-H. Kim, Y.-ll Jung, D.-J. Park, J.-Y. Park, Y.-H. Koo, Adhesion property and high-temperature oxidation behavior of Cr-coated Zircaloy-4 cladding tube prepared by 3D laser coating, J. Nucl. Mater. 465 (2015) 531–539.

[66] J.C. Brachet, M. Le Saux, M. Le Flem, S. Urvoy, E. Rouesne, T. Guilbert, C. Cobac, F. Lahogue, J. Rousselot, M. Tupin, P. Billaud, C. Hossepied, F. Schuster, F. Lomello, A. Billard, G. Velisa, E. Monsifrot, J. Bischoff, A. Ambard, ON-GOING STUDIES AT CEA ON CHROMIUM COATED ZIRCONIUM BASED NUCLEAR FUEL CLADDINGS FOR ENHANCED ACCIDENT TOLERANT LWRS FUEL, Proceedings of TopFuel 2015, (13-19 Sept. 2015), Zurich, Switzerland. (2015) 13–19.

[67] I. IDARRAGA-TRUJILLO, M. LE FLEM, J.-C. BRACHET, M. LE SAUX, D. HAMON, S. MULLER, V. VANDENBERGHE, M. TUPIN, E. PAPIN, E. MONSIFROT, A. BILLARD, F. SCHUSTER, Proceedings of TopFuel 2013, (13-19 Sept. 2013) Charlotte, North Carolina, USA, (2013) 860–867.

[68] V. Nieuwenhove, R., et al., In-pile testing of CrN, TiAlN and AlCrN coatings on Zircaloy cladding in the Halden Reactor, presented in 18th International Symposium on Zirconium in the Nuclear Industry. 2016: Hilton Head Island, SC, USA

[69] E. Alat, A. T. Motta, R. J. Comstock, J. M. Partezana, D. E. Wolfe, Ceramic coating for corrosion (c3) resistance of nuclear fuel cladding, Surface and Coatings Technology, 281 (2015) 133–143.

[70] U. Wiklund, P. Hedenqvist, S. Hogmark, B. Stridh, M. Arbell, Multilayer coatings as corrosion protection of Zircaloy, Surface and Coatings Technology, 86 (1996) 530–534.

[71] K. Daub, R. Van Nieuwenhove, H. Nordin, Investigation of the impact of coatings on corrosion and hydrogen uptake of Zircaloy-4, J. Nucl. Mater., 467 (2015) 260–270.

[72] S.S. Raiman, C. Ang, P. Doyle, K.A. Terrani, Hydrothermal Corrosion of SiC Materials for Accident Tolerant Fuel Cladding with and Without Mitigation Coatings, in: Springer, Cham, 2018: pp. 259–267.

[73] J. Braun, C. Guéneau, T. Alpettaz, C. Sauder, E. Brackx, R. Domenger, S. Gossé, F. Balbaud-Célérier, Chemical compatibility between UO2 fuel and SiC cladding for LWRs. Application to ATF (Accident-Tolerant Fuels), J. Nucl. Mater. 487 (2017) 380–395.

[74] C.M. Silva, Y. Katoh, S.L. Voit, L.L. Snead, Chemical reactivity of CVC and CVD SiC with UO_2 at high temperatures, J. Nucl. Mater. 460 (2015) 52–59.

[75] Gerczak, T.J., Discussion of potential fuel cladding chemical interactions in LWR designs utilizing SiC/SiC cladding, in 40th International Conference & Exposition on Advanced Ceramics & Composites. 2015: Daytona Beach, Florida, USA.

[76] D.J. Park, Y. II Jung, H.G. Kim, J.Y. Park, Y.H. Koo, Oxidation behavior of silicon carbide at 1200°C in both air and water-vapor-rich environments, Corros. Sci. 88 (2014) 416–422.

[77] V.A. Avincola, M. Grosse, U. Stegmaier, M. Steinbrueck, H.J. Seifert, Oxidation at high temperatures in steam atmosphere and quench of silicon carbide composites for nuclear application, Nucl. Eng. Des. 295 (2015) 468–478.

[78] Y. Lee, T.J. McKrell, A. Montecot, M. Pantano, Y. Song, M.S. Kazimi, Oxidation behavior of sintered tubular silicon carbide in pure steam I: Experiments, Ceram. Int. 42 (2016) 1916–1925.

[79] T. Cheng, J.R. Keiser, M.P. Brady, K.A. Terrani, B.A. Pint, Oxidation of fuel cladding candidate materials in steam environments at high temperature and pressure, J. Nucl. Mater. 427 (2012) 396–400.

[80] Y. Katoh, T. Koyanagi, J.L. McDuffee, L.L. Snead, K. Yueh, Dimensional stability and anisotropy of SiC and SiC-based composites in transition swelling regime, J. Nucl. Mater. 499 (2018) 471–479.

[81] T. Koyanagi, Y. Katoh, Mechanical properties of SiC composites neutron irradiated under light water reactor relevant temperature and dose conditions, J. Nucl. Mater. 494 (2017) 46–54.

[82] C.M. Petrie, T. Koyanagi, J.L. McDuffee, C.P. Deck, Y. Katoh, K.A. Terrani, Experimental design and analysis for irradiation of SiC/SiC composite tubes under a prototypic high heat flux, J. Nucl. Mater. 491 (2017) 94–104.

[83] L.L. Snead, S.J. Zinkle, D.P. White, Thermal conductivity degradation of ceramic materials due to low temperature, low dose neutron irradiation, J. Nucl. Mater. 340 (2005) 187–202.

[84] W. Primak, L.H. Fuchs, P.P. Day, Radiation damage in diamond and silicon carbide. Physical Review, 103(5), (1956) 1184.

[85] Y. Katoh, T. Nozawa, C. Shih, K. Ozawa, T. Koyanagi, W. Porter, L.L. Snead, High-dose neutron irradiation of Hi-Nicalon Type S silicon carbide composites. Part 2: Mechanical and physical properties, J. Nucl. Mater. 462 (2015) 450–457.

[86] T. Koyanagi, K. Ozawa, T. Hinoki, K. Shimoda, Y. Katoh, Effects of neutron irradiation on mechanical properties of silicon carbide composites fabricated by nano-infiltration and transient eutectic-phase process, J. Nucl. Mater. 448 (2014) 478–486.

[87] T. Koyanagi, Y. Katoh, K. Ozawa, K. Shimoda, T. Hinoki, L.L. Snead, Neutron-irradiation creep of silicon carbide materials beyond the initial transient, J. Nucl. Mater. 478 (2016) 97–111.

[88] Y. Katoh, L.L. Snead, T. Nozawa, S. Kondo, J.T. Busby, Thermophysical and mechanical properties of near-stoichiometric fiber CVI SiC/SiC composites after neutron irradiation at elevated temperatures, J. Nucl. Mater. 403 (2010) 48–61.

[89] G. Newsome, L.L. Snead, T. Hinoki, Y. Katoh, D. Peters, Evaluation of neutron irradiated silicon carbide and silicon carbide composites, J. Nucl. Mater. 371 (2007) 76–89.

[90] T. Koyanagi, Y. Katoh, J.O. Kiggans, T. Hinoki, H.E. Khalifa, C.P. Deck, C.A. Back, Irradiation resistance of silicon carbide joint at light water reactor–relevant temperature, J. Nucl. Mater. 488 (2017) 150–159.

[91] C.H. Henager, B.N. Nguyen, R.J. Kurtz, T.J. Roosendaal, B.A. Borlaug, M. Ferraris, A. Ventrella, Y. Katoh, Modeling and testing miniature torsion specimens for SiC joining development studies for fusion, J. Nucl. Mater. 466 (2015) 253–268.

[92] L. Goglio, M. Ferraris, Bonding of ceramics: An analysis of the torsion hourglass specimen, Int. J. Adhes. Adhes. 70 (2016) 46–52.

[93] W.G. Burns, P.B. Moore, Water radiolysis and its effect upon in reactor zircaloy corrosion, Radiat. Eff. 30 (1976) 233–242.